Collection MICROLOG sur Micromédia
Tableau de résolution

Droits d'auteurs

Les droits d'auteurs du conenu de cette microfiche sont détenus par l'éditeur du document original. Veuillez communiquer avec celui-ci pour obtenir des renseignements sur tout ce qui touche les droits d'auteurs. Les droits d'auteurs de cette édition sur microfiche sont détenus par Micromédia Limitée.

Qualité de reproduction sur microfiche

Micromédia Limitée maintient les normes de reproduction micrographique les plus élevées. Elle fait tout son possible pour obtenir la version sur papier à reproduire sur microfiche de la meilleure qualité possible. Cependant, certains styles d'imprimerie, de couleurs et de style de mise en page graphique (incluant des cartes, des grahiques et des tableaux) se reproduisent mal. En raison de la valeur du document original, Micromédia l'a reproduit tout en reconnaissant qu'il ne sera peut-être pas aussi lisable que le document original.

Tableau de résolution micrographique
National Bureau of Standards
Standard Reference Material 1010a
(ANSI and ISO Test Chart No. 2)

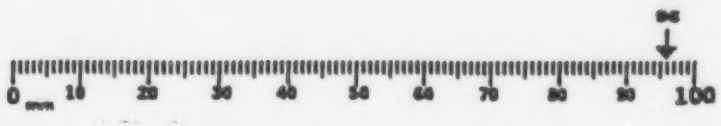

PM-1 3½"x4" PHOTOGRAPHIC MICROCOPY TARGET
NBS 1010a ANSI/ISO #2 EQUIVALENT

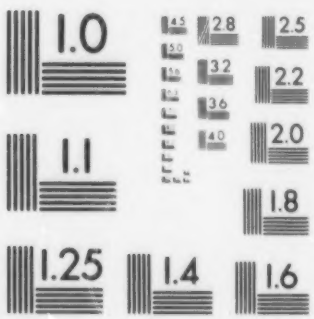

MS109

24x

NATIONAL MICROGRAPHICS ASSOCIATION

micromedia
a division of IHS Canada

20 Victoria Street, Toronto, ON M5C 2N8
Tel.: (416) 362-5211
Toll free: 1-800-387-2689
Fax: (416) 362-6161

FINAL REPORT

SINBAHD PROJECT:
INTEGRATION OF A LASER-INDUCED FLUORESCENCE LIDAR FOR THE DETECTION AND CHARACTERISATION OF THREATENING BIOLOGICAL CLOUDS

INO 99-5217SP RF N/A

Presented to:
PUBLIC WORKS AND GOVERNMENT SERVICES CANADA
Gare maritime Champlain
901 Cap Diamant
Québec (Québec) G1K 4K1

Prepared by:
Yves Painchaud, Ph.D.
Jean-François Cormier, Ph.D.
Jean-François Hébert, Ph.D.
Marc Deladurantaye, D.E.C.
Dimitri Antonov, M.Sc.
Brigitte Bélanger, M.Sc.
Sophie Bernier, M.Sc.
SCIENTIFIC AUTHORITY: J.R. Simard

Presented by:

Marc Levesque, M. Sc.
Project Manager

Authorized by:

Pierre Galarneau, Ph.D.
Director, Laser System Technologies

INO

May 2001

INO • 2740, rue Einstein, Sainte-Foy (Québec) Canada G1P 4S4

REPRODUCTION QUALITY NOTICE

This document is the best quality available. The copy furnished to DRDCIM contained pages that may have the following quality problems:

: Pages smaller or Larger than normal

: Pages with background colour or light coloured printing

: Pages with small type or poor printing; and or

: Pages with continuous tone material or colour photographs

Due to various output media available these conditions may or may not cause poor legibility in the hardcopy output you receive.

☒ If this block is checked, the copy furnished to DRDCIM contained pages with colour printing, that when reproduced in Black and White, may change detail of the original copy.

TABLE OF CONTENTS

1. Introduction **5**

2. System description **6**

2.1 Schematics of the optics 7

2.2 Main system parameters 8

2.3 Trailer installation 8

3. Processing and pre-processing **11**

3.1 Schematics of the emission and spectral channels 11

3.2 Pre-processing of the spectral signal 12

3.3 Determination of the bioaerosol concentration 15

3.4 Atmosphere attenuation 15

3.5 Pre-processing of the Backscatter signal 17

4. Software **19**

5. System characterization **20**

5.1 Steering mirror 20

5.2 Spectral channel 21

5.2.1 Telescope 21

5.2.2 UV Filters 22

5.2.3 Spectrometer 23

5.2.4 ICCD Camera 25

5.2 5 Delay generator 26

5.3 Backscattering channel 27

5.3.1 Licel transient recorder system 27

5 3.2 Beam splitter for the backscatter channel 27

5.3.3 Filter for the backscatter channel 28

5.4 Emission channel 28
5.4.1 Laser 28
5.4.2 Beam expander 35
5.4.3 Detector for optical triggering 35
5.4.4 Folding mirror 36
5.5 Visual channel 36
5.5.1 CCD Camera 36
5.5.2 Beam splitter for the visual channel 38
5.5.3 UV Filters 38
5.6 System synchronization 38
5.7 Overlapping functions 45
5.8 Weather monitoring (N.1, N.2, N.3, N.4, O.1) 48

6. Calibration 49
6.1 Data 49
6.2 Calibration procedure 50

7. Tests of the system in the field 51
7.1 Backscatter channel 51
7.1.1 Test with no target: Rayleigh scattering 51
7.1.2 Test with a solid target 54
7.2 Spectral channel 54
7.2.1 Background from day light 54
7.2.2 Signal from a solid target 56
7.2.3 Pre-processing and processing 59
7.2.4 Signal from the solid target placed at another distance 61
7.2.5 Raman signals 62

8. Alignment procedures 63
8.1 Changing the wavelength 63
8.1.1 Visual camera beam splitter 63
8.1.2 Visual camera UV filters 63
8.1.3 Spectrometer UV filters 63

8.1.4 UV transmitting filter for the backscatter channel 64

8.1.5 Beam expander 64

8.2 Weather station 64

8.3 Lidar alignment 64

8.3.1 Longitudinal position of the spectrometer 66

1. INTRODUCTION

The purpose of this document is to provide a description of an exploratory development model (XDM) of a laser induced fluorescence lidar system integrated into a trailer. The development of the XDM was done within the contract INO 5217 (DREV ref. W7701-8-3502/001/XSK in conformity with the proposal INO 98-5217 P N/A.

It is not the purpose of this document to provide the complete design description. The document rather gives a basic system description including the calibration data and alignment procedures.

The document INO 99-5217TS R N/A entitled "Sinbahd project: trailer specifications" was delivered in January 2000 and provides a more detailed description of the anticipated trailer fitting-out.

Although some basic description is given in the present document regarding the software, a more detailed description is presented in the XDM Software User Manual INO 99-5217SM R N/A.

A brief system description is presented in section 2. Section 3 describes the way the measured signals are processed before being displayed and for calculating the bioaerosol concentration. A brief description of the software is given in section 4 while the hardware is described in section 5. Section 6 relates to calibration. The tests performed in the field are described in section 7. Finally, the alignment procedures are given in section 8.

2. SYSTEM DESCRIPTION

The system described in this document is an exploratory development model (XDM) of a laser-induced fluorescence lidar integrated in a trailer. Its purpose is to remotely (50 m to 5000 m) detect and quantify the presence of fluorescent bioaerosols in suspension in the air. For that purpose, ultraviolet pulses of laser light are horizontally emitted in the air and a detection system collects the corresponding backscattered light that may contain a fluorescent component.

Laser pulses are emitted from an Excimer laser at either 308 or 351 nm coaxially with respect to the collection optics. The laser pulses are injected through a beam expander and a folding mirror, which form with the laser, the emission channel.

Part of the laser pulses emitted in the atmosphere is scattered back to the system and is collected by a 12"-diameter telescope and focused at the entrance slit of a spectrometer. A gated ICCD camera is used at the output port of the spectrometer to detect the spectral signature of a known fluorescent agent. The ICCD camera is gated such that only a probed cell located at a specific distance from the system is considered. Furthermore, the light entering the spectrometer is spectrally filtered to eliminate the light backscattered at the laser wavelength such that an eventual fluorescent component could be highlighted. Basically, the telescope, the spectrometer and the ICCD camera form the spectral channel.

Most of the light collected by the telescope is due to Rayleigh scattering in the air and is thus at the laser wavelength. This light is reflected to a photomultiplier tube connected to a transient recorder that records the detected intensity as a function of time with a time resolution in the order of 20 ns. The photomultiplier tube, the transient recorder and the telescope (shared with the spectral channel) form the backscatter channel, which is used to detect the presence of cloud along the system axis for distance varying between 50 and 5000 m.

Finally, a CCD camera records the image that can be seen through the emission channel. This allows visually observing the area under investigation. The CCD camera and its associated beam splitter form the visual channel.

A software controls the data acquisition, which are then processed for determining the bioaerosol concentration in the air. This aspect in described in more details in section 3.

2.1 Schematics of the optics

Figure 1 shows the schematics of the system optics. It also shows the presence of the steering mirror, which is used to control the angular position of the system axis (when properly aligned, the axes of the emission, spectral, backscatter and visual channels must be collinear).

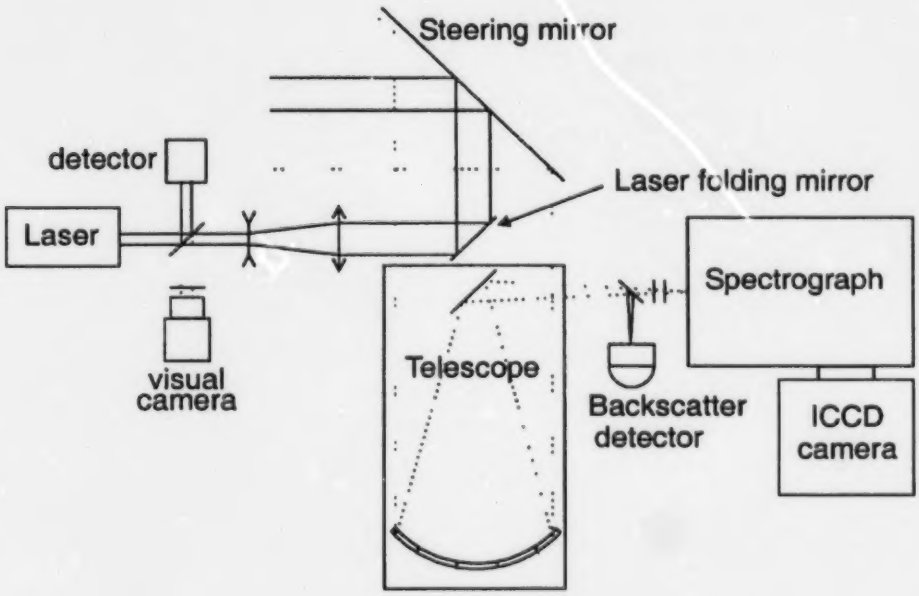

Figure 1: Schematics of the system optics.

2.2 Main system parameters

The main system parameters are the following:

- Beam expander magnification: 3.65
- Emission channel divergence: 69 µrad (H) × 72 µrad (H)
  (FWHM with magnification and pointing stability)
- Steering mirror displacement: ± 4° (both axes)
- Telescope clear aperture: 0.305 m (12")
- Telescope focal length: 1.27 m (50")
- Telescope F#: 4.2
- Telescope back focal length: 113.28 mm from flange (4.460")
- Spectrograph entrance slit width: 200 µm nominal (although the slit is adjustable)
- Spectrograph F#: 3.9
- Spectrograph span: 57 nm, 230 nm, 460nm (for grating 1,2 and 3)
- Spectrograph resolution: 1.2 nm, 4.8 nm, 9.6nm (for grating 1, 2 and 3)
- Spectral channel field of view: 157 µrad (H) nominal

2.3 Trailer installation

The system was mounted on a 4×8' optical table, itself installed at the rear of the trailer as shown in Figure 2. Figure 3 also shows a close top view of the geometric arrangement of the optical parts.

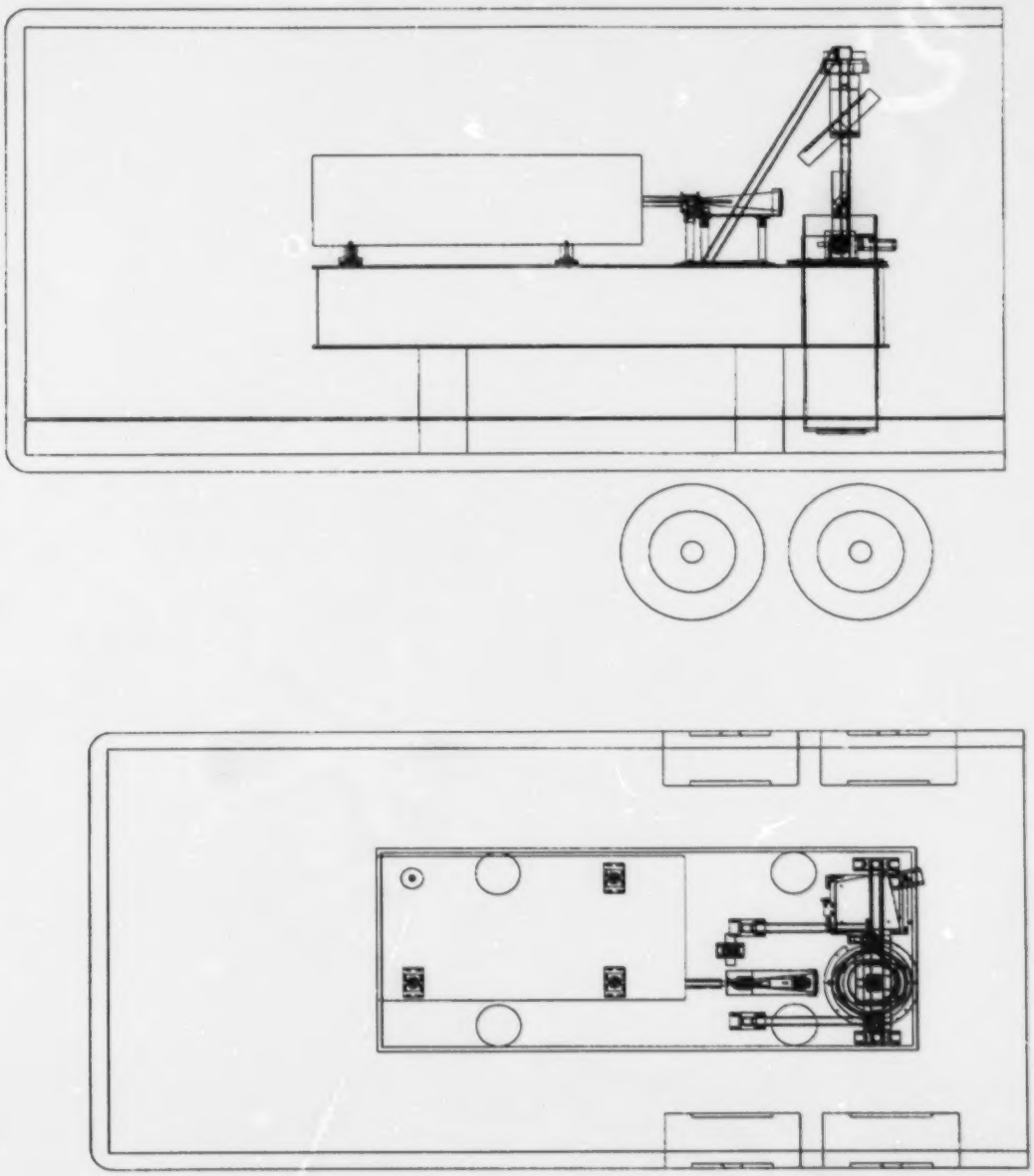

Figure 2: Schematics of the mechanical arrangement in the trailer.

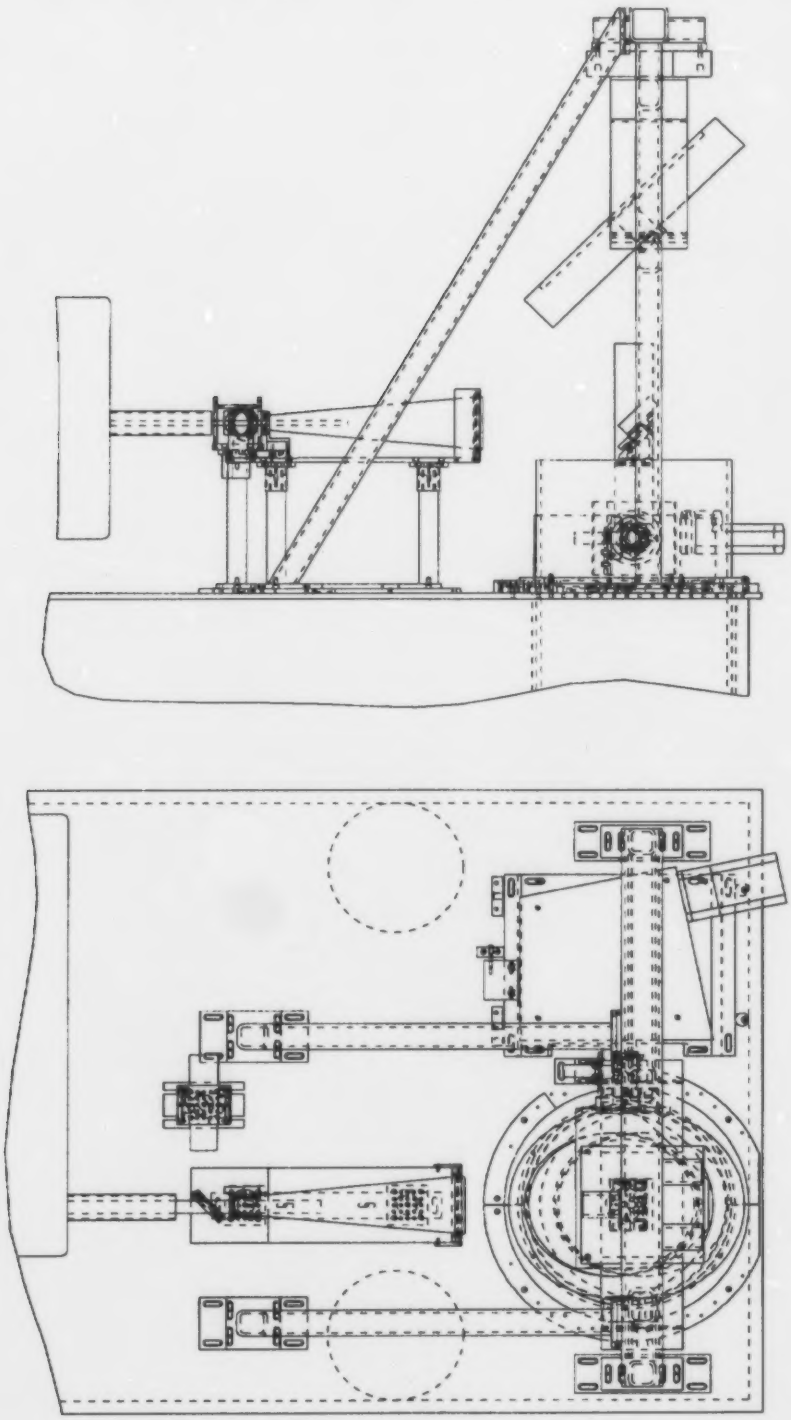

Figure 3: Close views of the geometric arrangement of the optical components.

3. PROCESSING AND PRE-PROCESSING

Basically, the critical information is measured through the spectral and backscatter channels. The raw data obtained from these two channels is pre-processed before being presented on the computer screen to the system user. This pre-processing basically consists in removing from the data the system dependent component in order to present to the system user data that rely only on the atmosphere behavior. Furthermore, a data processing is performed to extract the bioaerosol concentration.

The pre-processing of the spectral signal (measurement from the spectral channel) is done in such a way that all the system dependent components are removed and the information presented to the system user depends only on the atmosphere parameters at the probed cell location.

The pre-processing of the backscatter signal (measurement from the backscatter channel) does not remove all the system dependent component as no calibration is required for this signal. The pre-processing serves at removing the range-dependent component of the measured signal.

The pre-processed spectral signal is processed for obtaining the bioaerosol concentration at the probed cell location assuming a known spectral signature of the bioaerosol and using a fitting algorithm.

3.1 Schematics of the emission and spectral channels

The pre-processing of the spectral and backscatter signals rely on an appropriate knowledge of the system parameters.

The schematics presented in Figure 4 and Figure 5 show the different components of the injection and collection sub-systems respectively.

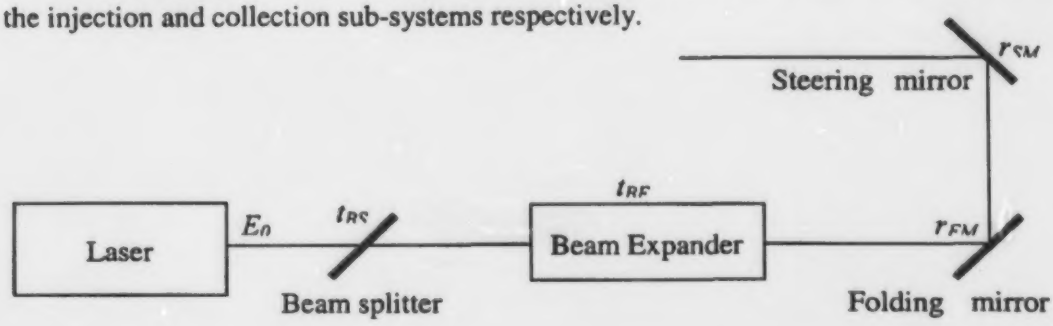

Figure 4: Injection sub-system

Referring to Figure 4, E_0 is the laser energy per pulse measured using the internal laser photodiode, t_{BS} is the transmittance of the visual camera beam splitter, t_{BE} is the transmittance of the beam expander, r_{FM} is the reflectance of the folding mirror and r_{SM} is the reflectance of the steering mirror.

The transmission of the injection optics $t_{oi}(\lambda)$ is given by:

$$t_{oi}(\lambda) = t_{BS}(\lambda) \cdot t_{BE}(\lambda) \cdot r_{FM}(\lambda) \cdot r_{SM}(\lambda). \quad (1)$$

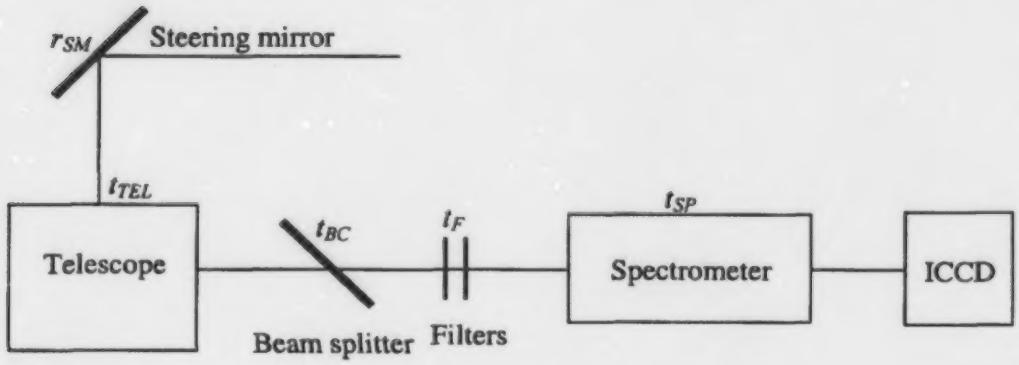

Figure 5: Collection sub-system

Referring to Figure 5, t_{TEL} is the telescope spectral transmission, t_{BC} is the transmission of the beam splitter for the backscattering channel, t_F is the transmission through the filters and t_{SP} is the transmission through the spectrometer.

Note that the telescope transmission t_{TEL} is the spectral transmission, which does not take into account the obscuration, vignetting and clipping. These geometric losses are rather taken into account by the geometric transmission factor $\xi(r)$.

The spectral transmission of the collection optics $t_{oc}(\lambda)$ is given by:

$$t_{oc}(\lambda) = r_{SM}(\lambda) \cdot t_{TEL}(\lambda) \cdot t_{BC}(\lambda) \cdot t_F(\lambda) \cdot t_{SP}(\lambda). \quad (2)$$

3.2 Pre-processing of the spectral signal

It is assumed that the ICCD camera provides a non-calibrated measurement $M(\lambda)$ of the spectrum. The measured signal $M(\lambda)$ is related to the spectral density of photons incident on the ICCD camera by a calibration vector $K(\lambda)$:

$$M(\lambda) = K(\lambda)\frac{dE}{d\lambda}(\lambda). \quad (3)$$

It is considered that the vector $M(\lambda)$ does not represent a direct measurement but rather a corrected measurement that includes a background subtraction. Also note that the calibration vector $K(\lambda)$ does not depend only on the wavelength λ but also on the voltage on the camera intensifier (the gain setting).

The vector $M(\lambda)$, obtained from the ICCD camera, is not directly a spectral measurement: it is rather a vector of responses obtained at each pixel of the camera. It can be correctly interpreted as a spectral measurement when the wavelengths corresponding to the pixels are known. The wavelength corresponding to a specific pixel depends on the grating type and on the grating angle inside the spectrometer. It is implicit that the vector $M(\lambda)$ contains as many elements as the number of ICCD camera pixels, where the wavelength λ could be explicitly written as:

$$\lambda = \lambda_{p,a,g}, \quad (4)$$

where the subscript p refers to the pixel number (varying from 1 to 674, the number of pixels), a refers to a specific grating angle (a certain number of accessible grating angles is predetermined) and g refers to the grating number (varying from 1 to 3). Equation (4) is the expression of the existence of a 3D wavelength calibration matrix. This calibration is more extensively discussed in section 5.2.4.

Assuming that the vector $M(\lambda)$ corresponds only to the fluorescence of bioaerosol having a concentration N_{ba}, it could be written as (from Simard *et al.*, Equation (2)):

$$M(\lambda) = K(\lambda)\ n_m E_0(\lambda_0)\Delta r\ \ \xi(r)\frac{A_0}{r^2}\ \ t_{oi}(\lambda_0)t_{oc}(\lambda)\ \ t_{ai}(\lambda_0,r)t_{ac}(\lambda,r)\ \ N_{ba}(r)\frac{d^2\sigma_{ba}}{d\Omega d\lambda}(\lambda_0,\lambda). \quad (5)$$

In this equation, the following quantities are assumed to be known:

$K(\lambda)$:	ICCD camera calibration function;
$\xi(r)$:	Geometric transmission factor of the collection system as a function of the range, taking into account the telescope obscuration, vignetting and clipping;
A_0:	Area over which the light is collected;
$t_{oi}(\lambda_0)$:	Transmission of the injection optics at the excitation wavelength λ_0 (also takes into account possible clipping)

$t_{oc}(\lambda)$: Spectral transmission of the collection optics at the wavelength λ (does not take into account the obscuration and other geometric losses);

$\frac{d^2\sigma_{bs}}{d\Omega d\lambda}(\lambda_0,\lambda)$: Spectral fluorescence differential cross section of the bioaerosol.

The following quantities are system parameters:

n_{pu}: Number of laser pulse within the measurement;

$E_0(\lambda_0)$: Energy of each pulse at the excitation wavelength λ_0;

Δr: Range resolution or probed cell thickness, assumed to be equal to $c/2(\tau_p+\tau_g)$ where τ_p is the laser pulse duration and τ_g is the gate duration;

r: Range (distance between the probed cell and the system).

Note that the quantities $t_{oi}(\lambda_0)$ and $t_{oc}(\lambda)$ also depend on the system parameters (excitation wavelength, spectrograph grating, grating angle).

Finally, the quantities $t_{ai}(\lambda_0,r)$ and $t_{ac}(\lambda,r)$ are the transmissions through the atmosphere of the injected and collected light respectively and are given by:

$$\begin{aligned} t_{ai}(\lambda_0,r) &= \exp(-\alpha(\lambda_0)\,r) \\ t_{ac}(\lambda,r) &= \exp(-\alpha(\lambda)\,r) \end{aligned}, \qquad (6)$$

where $\alpha(\lambda)$ is the attenuation of light at a wavelength λ propagating in the atmosphere. Section 3.4 discusses the way the atmosphere attenuation $\alpha(\lambda)$ is obtained.

It is useful to define the normalized spectral distribution $F(\lambda)$ as:

$$F(\lambda) = \frac{M(\lambda)}{K(\lambda)\;\; n_{pu}E_0(\lambda_0)\Delta r\;\; \xi(r)\frac{A_0}{r^2}\;\; t_{oi}(\lambda_0)t_{oc}(\lambda)\;\; t_{ai}(\lambda_0,r)t_{ac}(\lambda,r)}. \qquad (7)$$

The pre-processing of the spectral channel consists in calculating the normalized spectral distribution $F(\lambda)$ from the measured spectral signal $M(\lambda)$. The normalised spectral distribution $F(\lambda)$ does not depend on the system parameters but only on the atmosphere composition.

3.3 Determination of the bioaerosol concentration

In Equation (5), it was supposed that the spectral measurement corresponded only with the fluorescence of one type of bioaerosol. Taking into account the possible presence of one kind of bioaerosol and the Raman spectra of nitrogen and oxygen, and using the definition of the normalized spectral distribution $F(\lambda)$, Equation (5) is extended to:

$$F(\lambda) = N_{ba}(r)\frac{d^2\sigma_{ba}}{d\Omega d\lambda}(\lambda_0,\lambda) + N_N\frac{d^2\sigma_N}{d\Omega d\lambda}(\lambda_0,\lambda) + N_O\frac{d^2\sigma_O}{d\Omega d\lambda}(\lambda_0,\lambda), \qquad (8)$$

where N_N and N_O are the nitrogen and oxygen concentrations respectively.

Using the spectral differential cross sections for the bio-aerosol fluorescence and for the N_2 and O_2 Raman scattering, the quantities N_{ba}, N_N and N_O are obtained from a least mean square curve fit. The spectral differential cross section of the bio-aerosol fluorescence can be obtained from a measurement in known condition (known value of N_{ba}). The spectral differential cross-section of the Raman scattering of nitrogen and oxygen are known from the literature. The spectrally-integrated cross-sections are summarized in Table 1.

Molecule	Excitation wavelength	Raman scattering wavelength	Spectral width	Raman cross-section $d\sigma/d\Omega$
N_2	308 nm	331.82 nm	1.2 nm	5.18 E-30 cm^2/sr
	351 nm	382.27 nm	1.3 nm	2.94 E-30 cm^2/sr
O_2	308 nm	323.51 nm	1.2 nm	6.74 E-30 cm^2/sr
	351 nm	371.28 nm	1.3 nm	3.88 E-30 cm^2/sr

Table 1: Spectrally-integrated cross-section of the Raman scattering for nitrogen and oxygen.

3.4 Atmosphere attenuation

The spectral atmosphere attenuation $\alpha(\lambda)$ is obtained using a certain atmospheric model and the attenuation value α_{ref} at a single wavelength λ_{ref}. In other words, assuming that the atmospheric attenuation is known at one wavelength, it can be deduced for other wavelengths using an atmospheric model.

In the software, it appears useful to define a function ATMOSPHERE that would incorporate an atmospheric model and that would take as input data the wavelength at which the attenuation has to be calculated, a certain reference wavelength, and the atmospheric attenuation at the reference wavelength. Then, the attenuation at an arbitrary wavelength λ will be calculated using:

$$\alpha(\lambda) = \text{ATMOSPHERE}(\lambda, \lambda_{ref}, \alpha_{ref}). \quad (9)$$

In such a way, it could be easy to change the atmospheric model by another one. Within the framework of the project at INO, only the Kruse model will be used.

Function ATMOSPHERE (λ, λ_{ref}, α_{ref}) which incorporates the Kruse model can be simply written as:

$$\text{ATMOSPHERE}(\lambda, \lambda_{ref}, \alpha_{ref}) = \alpha_{ref}\left(\frac{\lambda_{ref}}{\lambda}\right)^{q}, \quad (10)$$

where $q = 1.3$.

The value α_{ref} can be determined for $\lambda_{ref} = 875$ nm using the visibility monitor which can output both the visibility value V_M or the atmospheric attenuation α.

The value α_{ref} can also be determined from the Raman signals of the nitrogen and/or oxygen. Instead of being applied to $F(\lambda)$, the curve fit procedure is applied to $F(\lambda) \cdot t_{at}(\lambda_0, r) \cdot t_{ac}(\lambda, r)$ which results in obtaining the curve fit parameters N_N' and N_O' given by:

$$N_N' = N_N \cdot t_{at}(\lambda_0) \cdot t_{ac}(\lambda_{RN}), \quad (11)$$

$$N_O' = N_O \cdot t_{at}(\lambda_0) \cdot t_{ac}(\lambda_{RO}), \quad (12)$$

where N_N and N_O are the known nitrogen and oxygen concentrations of air ($N_N = 0.78084 \cdot N$ and $N_O = 0.20947 \cdot N$, where $N = 2.5401 \times 10^{15}$ molécules/cm$^3 \cdot e^{-0.0001\,z}$ is the dry air concentration at altitude z) and where λ_{RN} and λ_{RO} are the wavelengths of the Raman scattering from the nitrogen and oxygen respectively.

Combining Equations (6), (9), (11) and (12), one obtains:

$$\alpha_{RN} = -\frac{1}{r}\ln\left(\frac{N_N'}{N_N}\right)\left(1+\frac{1}{\alpha_{RN}}\text{ATMOSPHERE}(\lambda_0, \lambda_{RN}, \alpha_{RN})\right)^{-1}, \quad (13)$$

$$\alpha_{RO} = -\frac{1}{r}\ln\left(\frac{N'_O}{N_O}\right)\left(1+\frac{1}{\alpha_{RO}}\,\mathrm{ATMOSPHERE}(\lambda_0,\lambda_{RO},\alpha_{RO})\right)^{-1}. \quad (14)$$

The values for α_{RN} and α_{RO} are obtained by solving Equations (13) and (14). One of these attenuation values can than be used as α_{ref}. Note that Equation (13) and (14) are transcendental equations that may require an iterative procedure. For the particular case of function ATMOSPHERE incorporating the Kruse model, the transcendental character of Equations (13) and (14) disappear as function ATMOSPHERE depends linearly on the reference attenuation.

Although it does not appear explicitly, when λ_{ref} and α_{ref} are determined from the Raman signal, possible system calibration inaccuracies are compensated for, especially when the same range is used for both the Raman and fluorescence signals. It is easy to show that, when using the Raman signal for characterizing the atmosphere, the one from the nitrogen for example, the bioaerosol concentration should correspond to:

$$N_{ba} = N_N \frac{M_F(\lambda,r)}{M_{RN}(\lambda_{RN},r_{RN})} \frac{\left(\frac{d^2\sigma_N}{d\Omega d\lambda}\right)}{\left(\frac{d^2\sigma_{ba}}{d\Omega d\lambda}\right)} \frac{C(\lambda_0,\lambda_{RN},r_{RN})}{C(\lambda_0,\lambda,r)}, \quad (15)$$

where $M_F(\lambda, r)$ is the fluorescence signal measured at wavelength λ and at a range r, $M_{RN}(\lambda_{RN}, r_{RN})$ is the nitrogen Raman signal measured at wavelength λ_{RN} and at a range r_{RN} and $C(\lambda_0, \lambda, r)$ is the overall calibration function given by:

$$C(\lambda_0,\lambda,r) = K(\lambda)\; n_{pu} E_0(\lambda_0)\Delta r\; \xi(r)\frac{A_0}{r^2}\; t_{oi}(\lambda_0)t_{oc}(\lambda)\; t_{oi}(\lambda_0,r)t_{oc}(\lambda,r). \quad (16)$$

Equation (15) indicates that using the Raman signal for characterizing the atmosphere attenuation, the determination of the bioaerosol concentrations should depend only weakly on the system and calibration parameters, especially when ranges r and r_{RN} are close and when the fluorescence and Raman wavelengths λ and λ_{RN} are close.

3.5 Pre-processing of the Backscatter signal

In the backscatter window, the signal obtained from the Transient Recorder (Licel system) is displayed as a function of the range r after some corrections being applied. The

raw signal is for the range ($1/r^2$ and system dependence as a function of the range), the laser energy and the atmospheric transmission. This can be written as:

$$P_{bs}(r) = M_{bs}(r)\frac{r^2}{\xi_{bs}(r)\, n_{pu}\, E_0\, t_{an}^2(\lambda_0)}, \tag{17}$$

where $M_{bs}(r)$ is the raw measurement and $P_{bs}(r)$ is the displayed function. Note that $P_{bs}(r)$ is expressed in arbitrary units. Note also that $\xi_{bs}(r)$ is different from $\xi(r)$ in Equation (5), $\xi(r)$ includes the geometric transmission through the spectrometer while $\xi_{bs}(r)$ includes the geometric coupling to the Licel detector.

4. SOFTWARE

Software installed in primary computer controls all the instruments except the steering mirror, which is controlled via a secondary computer and/or a joystick. The software assures proper synchronization between the instruments, acquires the data, perform pre-processing and processing resulting in obtaining a bioaerosol concentration in a probed atmosphere cell.

The software manages the data acquisition following four different modes of operation:

- Single acquisition
- Multiple acquisition
- Search and track
- Surveillance and track

These modes of operation, as well as the general software operation, are discussed in more details in the Software User Manual INO 99-5217SM R N/A.

5. SYSTEM CHARACTERIZATION

The characterization of the different system components is presented in the following sections. The components are classified as a function of the channel in which they are. Some components have been associated to one channel even they are also part of another one.

The steering mirror is not associated to a specific channel as it is involved in each of them. The equipment for weather monitoring is also presented in a separate section.

In addition to the characterization of individual components, the system synchronization and the overlapping functions are presented in this section. The overlapping functions take into account the spatial profile and the divergence of the laser beam and give an evaluation of the whole system geometric transmittance (as opposed to optical transmittance). When calculating the overlapping functions, obscuration, vignetting and clipping at both the injection and collection optics are taken into account.

The information provided in this section basically consists in a description of the system components. Component characteristics are also given, especially when they are required as part of the calibration data. Some test results are also given as a verification of a proper operation.

5.1 Steering mirror

The steering mirror (provided by DREV) is a flat $\lambda/10$ mirror coated with MgF_2. It is from Stabilite Cellular Mirrors and has the reflectivity curve from 300 to 600 nm shown in Figure 6. This reflectivity curve was provided by the manufacturer, with no mention on the angular incidence which is expected to be very weak. The steering mirror has been mounted in a gimbal model AOM130M-400-2-41 from Aerotech (also provided by DREV) which allow angular displacements of ±4° in both axes with resolution of 0.037 arc sec and repeatability of 0.75 arc sec. The mirror reflectivity is 0.895 at 308 nm and 0.903 at 351 nm.

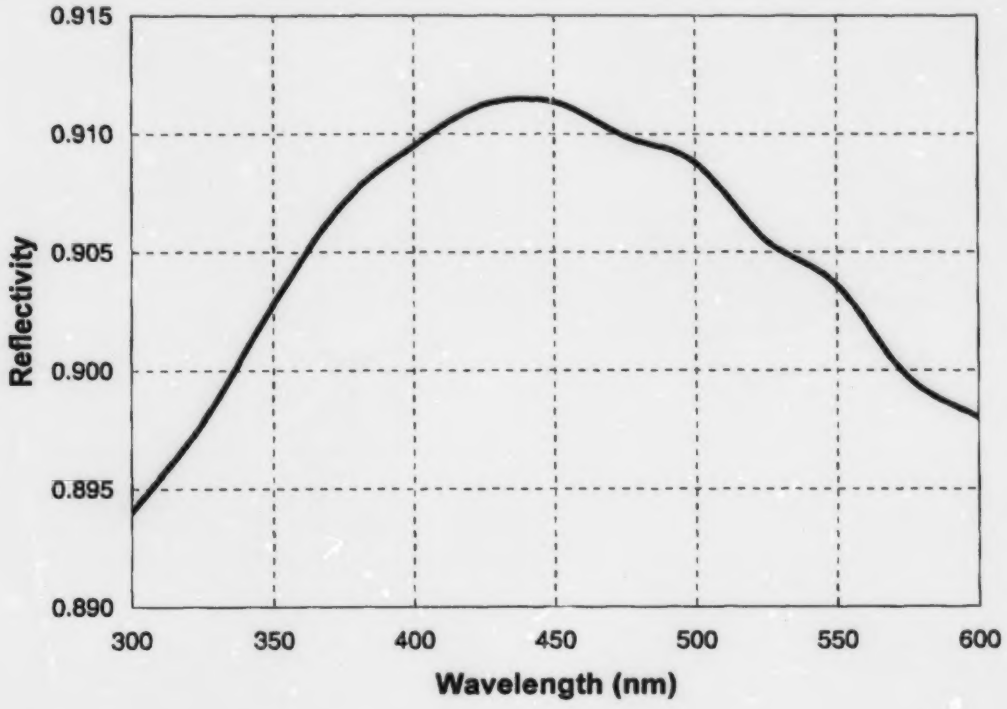

Figure 6: Reflectivity curve of the steering mirror.

5.2 Spectral channel

5.2.1 Telescope

The telescope, a major part of the collecting system, is a newtonian telescope from SORL. It is composed of a large parabolic mirror and a small flat mirror. It has a focal length of 1.2704 m (50.017") and a clear aperture of 0.3048 m (12.000"). The transmittance of the telescope between 300 and 600 nm is shown in Figure 7. The transmittance is 0.80 at 308 nm and 0.86 at 351 nm. The curve shown in Figure 7 has been obtained from the witness reflectivity data provided by the manufacturers. The data from 250 and 350 nm have been provided as well as from 420 to up to 2500 nm. The data between 350 and 420 nm have been interpolated.

The telescope is partly obscured by its folding mirror and corresponding holder and spider and also by the laser-folding mirror. The overall telescope obscuration is 0.101.

This number has been evaluated geometrically based on the measurement of the dimensions of the elements located within the telescope area.

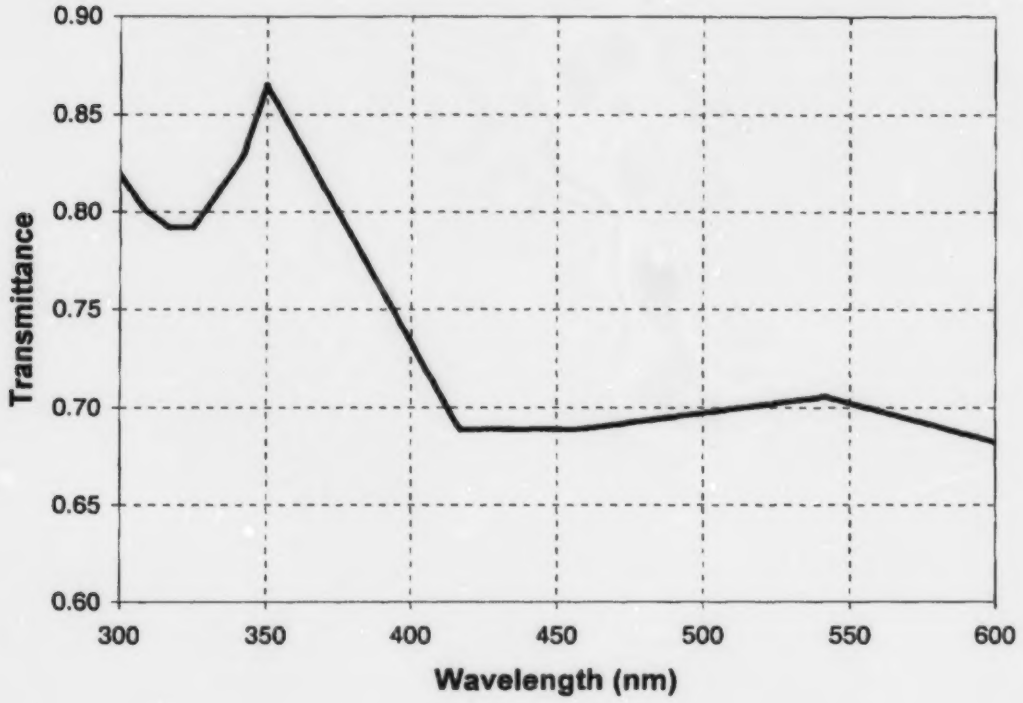

Figure 7: Transmittance of the telescope between 300 and 600 nm.

5.2.2 UV Filters

Four identical filters are used in the system to eliminate laser radiation. Two are placed in front of the spectrometer and two are placed in front of the visual camera. The filters must transmit Raman signals however. The four filters must be replaced when changing the wavelength: the GG375 filters must be used for 351 nm operation while the WG335 are used for 308 nm operation. The transmittance of the filters is presented in Figure 8.

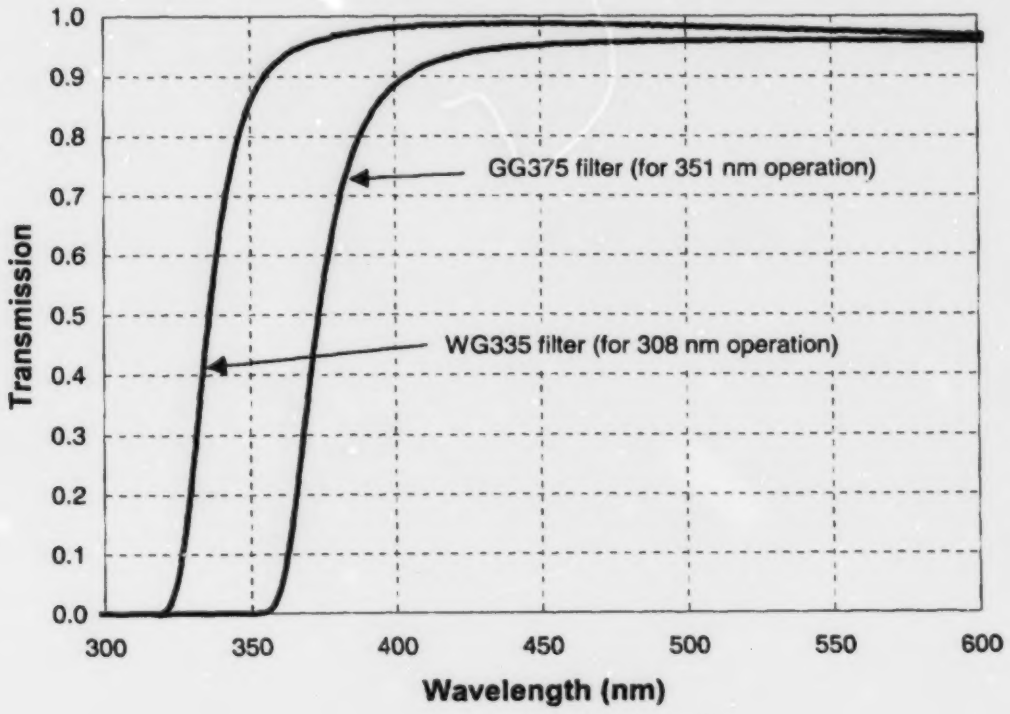

Figure 8: Transmittance of the UV filters.

5.2.3 Spectrometer

The spectral information of the collected light is analyzed using a spectrometer model MS260i from Oriel. It has three gratings that can be remotely changed and adjusted. The grating characteristics are given in Table 2. A slit of adjustable width is used as the entrance port although the system is designed to be used with a slit width value of 200 µm. The variable width slit provides a greater flexibility which is also required. Figure 9 shows the slit width as a function of the micrometer reading. According to this characterization, the micrometer must be adjusted to 213 µm in order for the slit to have an actual aperture of 200 µm.

Grating	Lines par mm	Resolution	Span
1	1200	1.2 nm	57 nm
2	300	4.8 nm	230 nm
3	150	9.6 nm	460 nm

Table 2: Description of the three Spectrometer gratings.

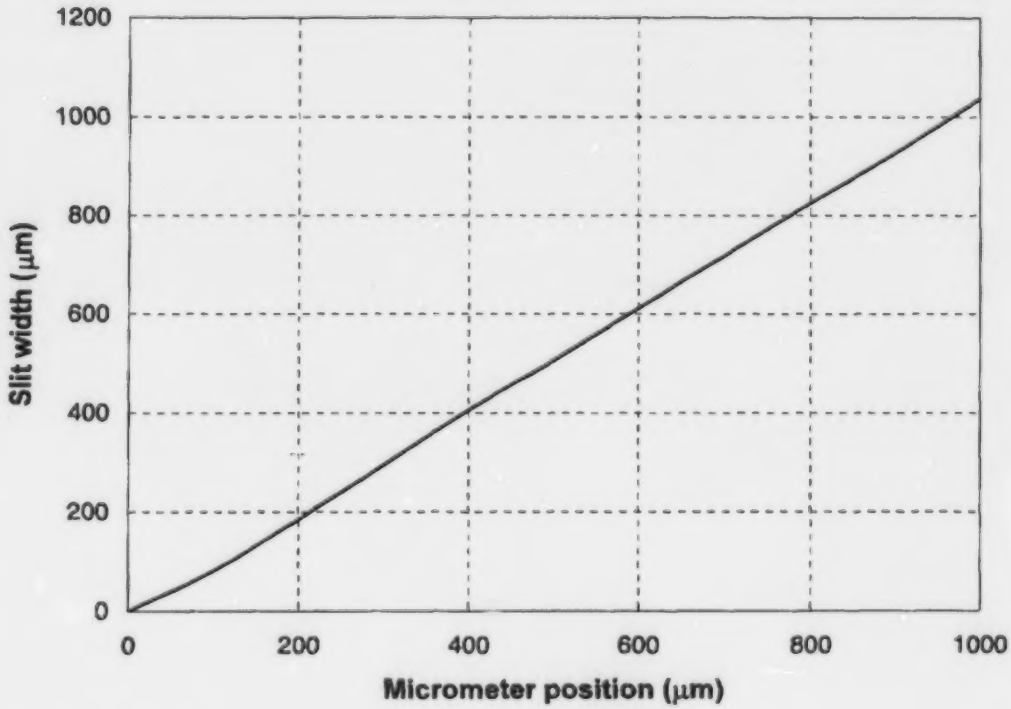

Figure 9: Entrance slit width as a function of the micrometer reading.

The wavelength calibration of the spectrometer is related mainly to the grating characteristics. However, since it depends also on the geometry of the detector placed at the output port (i.e. the ICCD camera), this point is addressed in the following section.

As discussed in section 3, the spectrometer transmittance $t_{SP}(\lambda)$ has to be determined. However, the spectrometer transmittance has been determined together with the ICCD camera response. Thus, this point is also addressed in the next section.

5.2.4 ICCD Camera

An ICCD model DH501-18F-01 (option W) from Andor Technologies is placed at the output of the Oriel spectrometer. The CCD camera is 1024 pixels (width) by 128 pixels (height). The physical width of the CCD camera is 1 inch while the intensifier is smaller (18 mm) such that only 674 pixels are intensified and actually useful. The intensifier can be gated in the nanosecond range using a fast TTL signal. The actual gate aperture is 12 nanoseconds less than the width of the TTL signal.

Obviously, the images measured by the CCD can be transferred to the computer. However, on-board pixel summing, referred to as binning, can be done before the data being transferred. In our application, a full vertical binning (perpendicular to wavelength dispersion) was done allowing for a fast data transfer. Then, only vectors, that contains the spectral information, were transferred to the computer. It is important to know to which wavelength corresponds each of the vector element. This association between the wavelength and the vector number consists in the wavelength calibration of the spectrometer-ICCD combination.

As discussed in section 3.2, the association pixel-wavelength depends on the grating used in the spectrometer and on its angle resulting in Equation (4).

Also discussed in section 3.2, the signal $M(\lambda)$ measured with the ICCD camera is related to the spectral density of energy incident on the camera $dE/d\lambda$ by:

$$M(\lambda) = K(\lambda)\frac{dE}{d\lambda}(\lambda). \tag{18}$$

A similar equation can be written to relate the measured signal $M(\lambda)$ with the spectral density of energy entering into the spectrometer $dE_0/d\lambda$. This can be written as:

$$M(\lambda)=t_{SP}(\lambda)K(\lambda)\frac{dE_0}{d\lambda}(\lambda), \tag{19}$$

where obviously the spectrometer transmittance is taken into account. For practical reason, the product $t_{SP}(\lambda)\cdot K(\lambda)$ is determined as a single parameter and the single quantities $t_{SP}(\lambda)$ and $K(\lambda)$ remain unknown. More precisely, this product has been determined in the specific case of having the maximum gain setting on the ICCD. It is assumed that the different intensifier gain settings affects all the pixels in the same manner such that the product $t_{SP}(\lambda)\cdot K(\lambda)$ can be properly written as:

$$t_{SP}(\lambda)\, K(\lambda) \;=\; \kappa(\lambda)\, G\,, \qquad (20)$$

where $\kappa(\lambda)$ is the product $t_{SP}(\lambda)\cdot K(\lambda)$ when the maximum gain setting is used and G is a correction factor for other gain settings. These correction gain factors are given in Table 3.

Gain setting	Correction gain factor G
0	0.000567
1	0.00178
2	0.00548
3	0.0108
4	0.0388
5	0.0571
6	0.0875
7	0.116
8	0.922
9	1

Table 3: Intensifier gain of the ICCD camera relative to the maximum gain setting.

5.2.5 Delay generator

The delay generator is required to synchronize the ICCD gated measurement with the laser pulses with a specified time interval which define the distance of the probed atmospheric cell under instigation. The XDM uses a delay generator model DG535 from Stanford Research Systems capable of delaying the signals by a time interval up to 1000 s with a resolution of 5 ps. The proper operation of the delay generator was verified during the field tests.

5.3 Backscattering channel

5.3.1 Licel transient recorder system

The backscatter signal is measured using the Lidar transient recorder from Licel GbR. This supplier provides an integrated system that includes a photomultiplier tube model R7400-06 from Hamamatsu and all the related supply, ultrafast electronics, and boards for communication with a PC. The bin width is 25 ns and signal length can be up to 200 μs, which corresponds to 30 km. The Licel system provides signals in both analogic and photon counting modes, simultaneously. The Sinbahd Software properly mix those two signals. The PMT voltage is adjusted manually from 0 up to 800 V on the Licel controller.

The sensitive area of the PMT, once installed in its mount, is circular with a diameter of 8 mm.

The test of the Licel system has been done in the field (see section 7.1).

5.3.2 Beam splitter for the backscatter channel

A beam splitter directs part of the light focused by the telescope on the sensitive area of the Licel PMT. The beam splitter does not make any wavelength filtering, it rather direct a small fraction of the light (which is mainly at the laser wavelength) to the PMT.

Since the backscatter channel is not required to be calibrated, the reflectivity of the beam splitter was not determined. Its transmittance between 300 and 600 nm was important however since it affects the spectral channel calibration. The transmittance of the beam-splitter is shown in Figure 10.

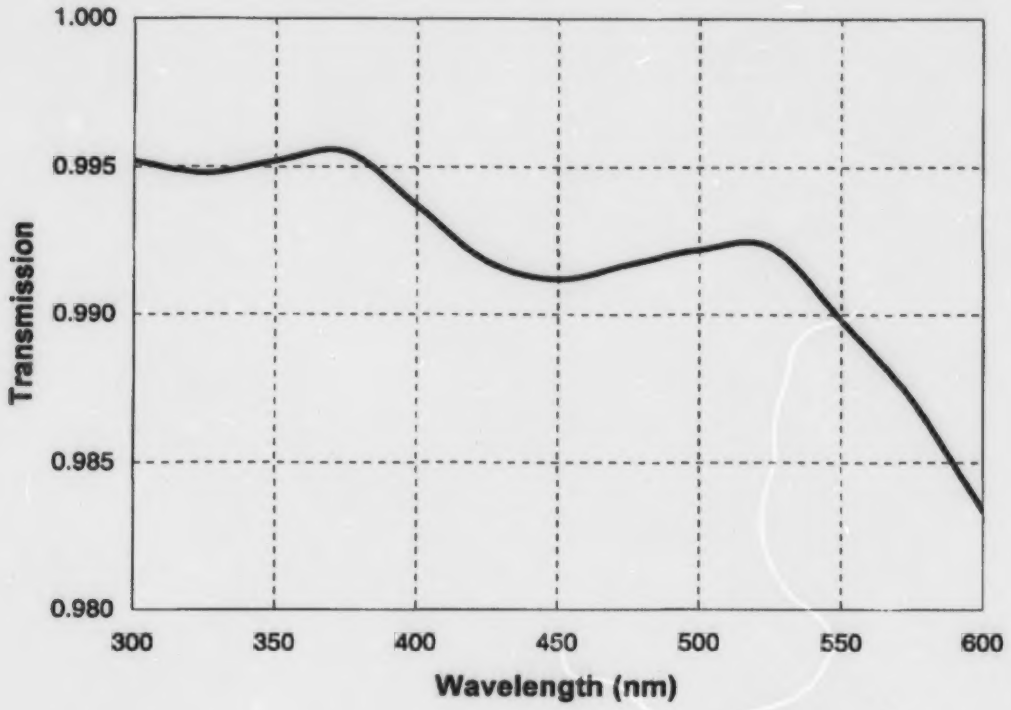

Figure 10: Transmittance of the backscatter channel beam splitter between 300 and 600 nm.

5.3.3 Filter for the backscatter channel

A filter is placed in front of the Licel detector to remove light at wavelength different from the laser wavelength. The filter is from CVI Laser Corp. and has a spectral width of 10 nm. The filter model F10-350.0-4-0.5 centered at 350 nm is used for the laser operation at 351 nm. The filter model F10-307.1-3-0.5 centered at 307.1 nm is used for the laser operation at 308 nm.

5.4 Emission channel

5.4.1 Laser

The laser source is an Excimer laser model PM-848 with an unstable resonator from GSI Lumonics. It has the possibility of being operated with XeF (with an emission wavelength

of 351 nm) or with XeCl (with an emission wavelength of 308 nm). Changing the gas type appears feasible although it is strongly discouraged by GSI Lumonics. During the laser installation, Steve Hastie from Lumonics suggested that buying another laser vessel (its cost is about 30 000$) specifically for operation with XeCl could be a good approach: changing the laser vessel appears feasible on the field by the peoples from DREV. The specifications of the laser are listed in Table 4. Many of the laser characteristics are of primary importance for the XDM calibration.

	Lumonics PM-848 with unstable resonator	
	With XeF	With XeCl
Wavelength	351 nm	308 nm
Average power	25 W	25 W
Maximum repetition rate	200 Hz	200 Hz
Beam size	25 × 10 mm	25 × 10 mm
Beam divergence	< 300 μrad	< 300 μrad
Pointing stability	< 200 μrad	< 200 μrad
Gas lifetime	> 20×10^6 shots	> 8×10^6 shots

Table 4: Specifications of the PM-848 excimer laser.

a) Output power

During the installation of the laser, pulses as strong as 200 mJ have been generated at a repetition rate of 200 Hz, corresponding to an average power of more than 40 W. This value decreases as the gas degrades.

b) Pulse duration

The duration of the laser pulse has been measured using the detector used for optical trigging, which has a rise time of the order of a nanosecond.. The resulted signal is shown in Figure 11 showing duration of 15.1 ns (FWHM).

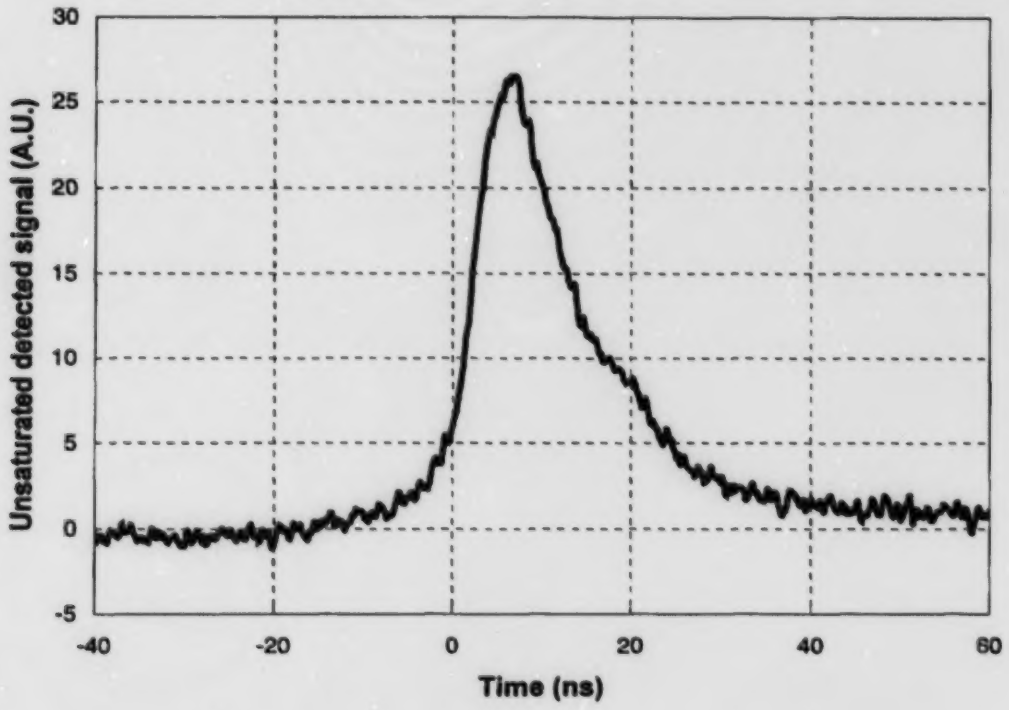

Figure 11: Temporal distribution of the laser pulse.

c) Beam size

The image of the spatial profile was measured at the laser output. This image is shown in Figure 12. Obviously, the optical quality is very poor as the cavity is optimized for far field quality instead of near field. The spatial profile has been measured at a distance of 23 cm from the laser case when operated at 33 kV. Although, the laser is more likely to be operated at 30 kV, the profile at 33 kV is shown as being the worst case. The near field quality varies only weakly on the pump level anyway. One dimension profiles are also shown in Figure 13 for both vertical and horizontal axes.

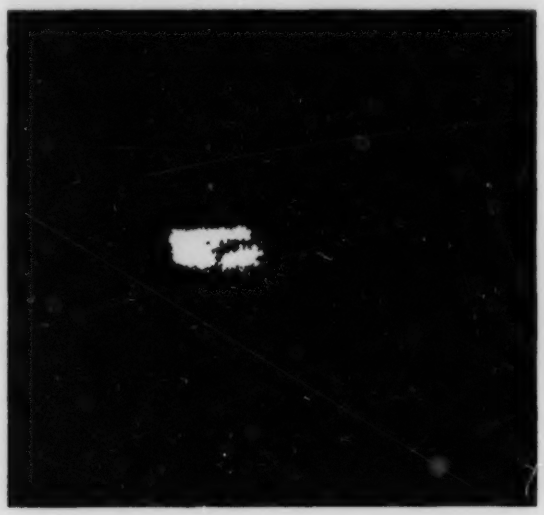

Figure 12. Near-field profile (23 cm from the laser case) when operated at 33 KV.

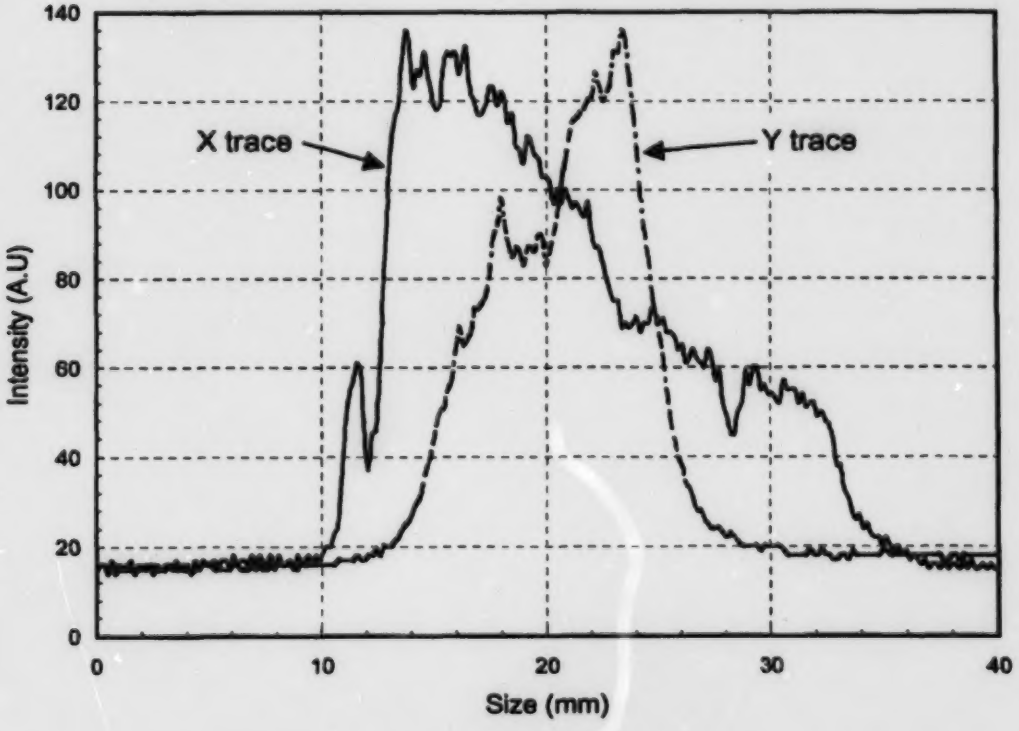

Figure 13: X and Y traces of the image shown in Figure 12.

From the spatial distribution shown in Figure 12, the beam size was determined. More precisely, the minimum rectangles containing 90%, 95%, and 99% were determined. The results are summarized in Table 5.

Fraction of the energy	Beam size (H × V)
90%	21.5 mm × 10.9 mm
95 %	22.5 mm × 12.3 mm
99 %	24.0 mm × 14.3 mm

Table 5: Beam size as defined as a rectangle containing a certain proportion of the laser energy.

d) Beam divergence and pointing stability

The beam divergence and pointing stability have been determined from the characterization of the far field spatial distribution, that is, the spatial distribution at the focal plane of a lens. The laser was operated at 30 kV and 1Hz repetition rate during this measurement. Figure 14 shows the contour profile while

Figure 15: X and Y traces of the image shown in Figure 14.

shows the one dimension profiles in both horizontal and vertical directions.

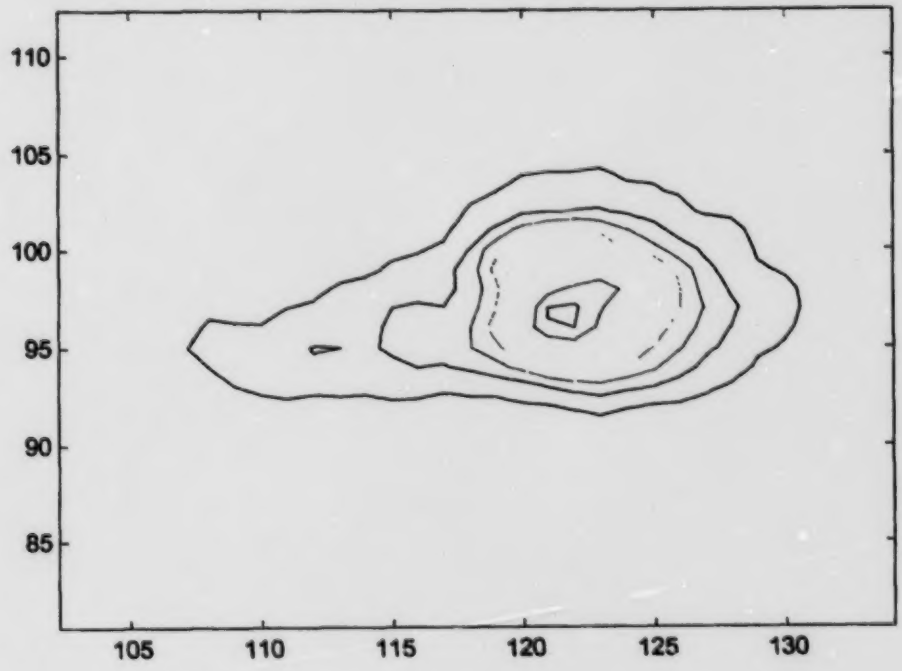

Figure 14: Far-field profile when the laser is operated at 33 KV. The axes are in pixels (33 μrad/pixel).

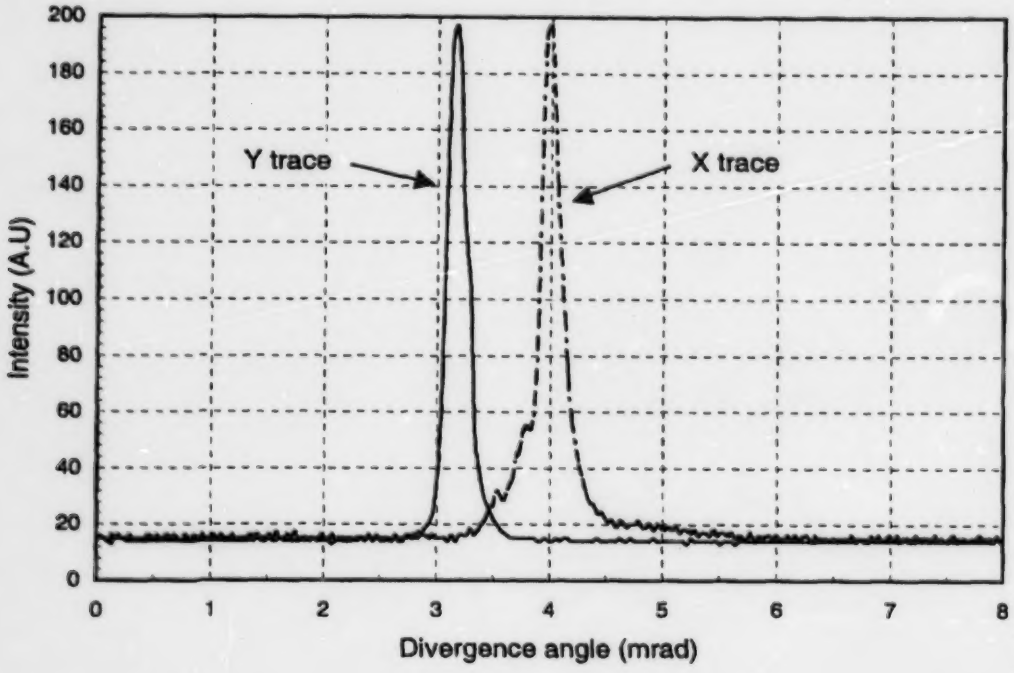

Figure 15: X and Y traces of the image shown in Figure 14.

The beam divergence in both axes was determined by analyzing the X and Y traces shown in Figure 15. From these curves, two values were calculated: the full width at half maximum (FHWM) and the standard deviation defined as $\sigma_2 = \sqrt{\left\langle \left(x - \langle x \rangle\right)^2 \right\rangle}$ where <x> is the abscissa average with ordinate weighting. The standard deviation is calculated in one dimension, i.e. on the X and Y traces. This calculation is very sensitive on the background noise: an appropriate DC level was subtracted and the values under a certain threshold were ignored in order to minimize the contribution of the background noise. The resulting values are given in Table 6.

	FWHM (μrads)	σ_2 (μrads)
X (horizontal)	198 ± 17	297 ± 17
Y (vertical)	208 ± 17	112 ± 17

Table 6: FWHM and σ_2 of the X and Y beam divergences.

It can be observed, from both the data of Table 6 and from Figure 14, that the divergence is spread more is the X-axis than it is in the Y-axis. In fact, a Gaussian distribution would have a standard deviation σ_2 2.355 times smaller than its FWHM. This is obviously not the case for the horizontal profile and this is due to the strong wings of the divergence profile in this axis.

The pointing stability was also evaluated. Over 152 pulses (at 1 Hz), a standard deviation of ± 17 µrads was observed with maximal excursion of ± 53 µrads.

5.4.2 Beam expander

The beam expander is composed of two lenses. The first one is a UV-coated spherical plano-concave fused-silica lens model PLCC-38.1-77.3-UV-248-355 from CVI Laser Corporation. The second one is a custom plano-convex fused silica lens (quote Q9730) from Optimax that has been UV-coated (BBAR coating) by GSI Lumonics. The manufacturers provided data on the coating reflectivity. It is assumed that the attenuation within the material, less than 0.1% can be neglected. Considering the surface reflections, the beam expander transmittance has been evaluated. The lens and beam expander parameters are given in Table 7. The first lens is mounted on a translation stage that can be adjusted with a micrometer.

Wavelength	First lens focal length	Second lens focal length	Distance between lenses	Beam expander magnification	Beam expander transmission
308 nm	-159 mm	581 mm	414.90 mm	3.653	0.996
351 nm	-162 mm	592 mm	422.72 mm	3.652	0.996

Table 7: Lens focal lengths and beam expander magnification at 308 and 351 nm.

5.4.3 Detector for optical triggering

A photodiode detector model FDS010 (TO5) from Thorlabs is used for optically triggering the light collection devices. Home maid electronics is used to provide two identical output TTL signals suitable for triggering the Licel system and the SRS delay generator. Figure 16 shows a typical output of the electronic board associated with the triggering detector. A more completed description of the operation of this sub-system is discussed in section 5.6.

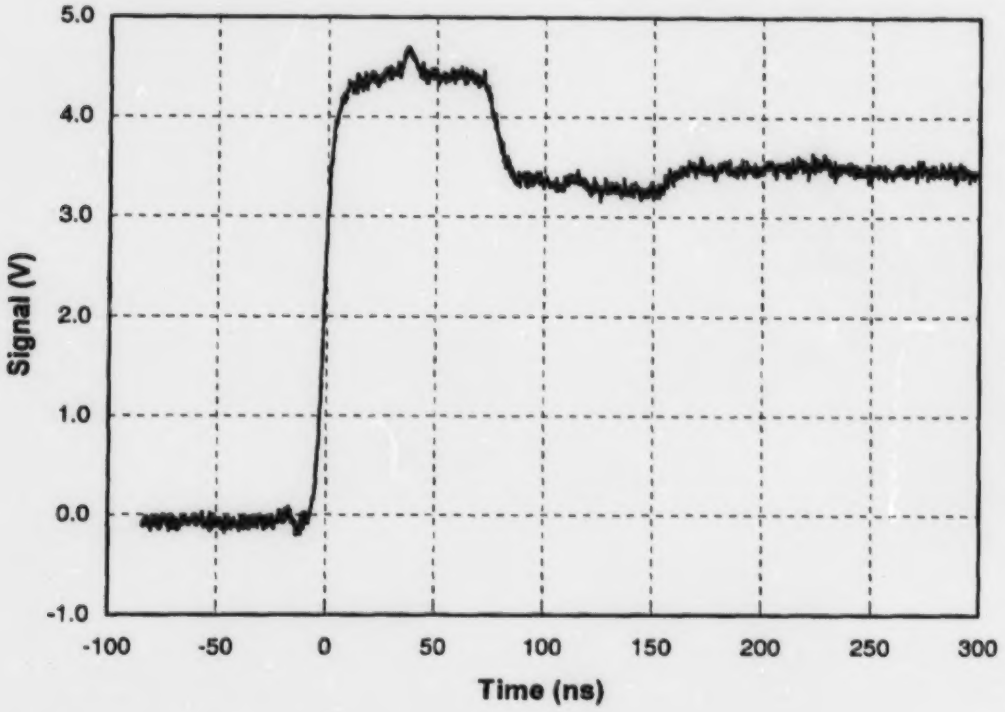

Figure 16: Typical signal obtained at the trigger detector.

5.4.4 Folding mirror

The folding mirror is a UV-coated aluminum mirror model MPS 14430/302 from JML Optical Industries. It has a reflectivity of 92% at both 308 and 351 nm. The folding mirror clips part of the laser beam. This clipping is taken into account by the overlapping functions, as discussed in section 5.7.

5.5 Visual channel

5.5.1 CCD Camera

A CCD Camera model SONSPT-M314 from Sony is used for viewing the area under inspection. The camera has been selected for meeting the requirement of visualizing 200 times the field of view of the spectral channel. The required field of view of the CCD camera is thus 31.4 mrad. The chosen camera is equipped with a zoom lens that can be adjusted to have a field of view of 31.4 mrad.

The field of view of the CCD has been verified by placing an object of known size at a known distance from the system. A 8½×11 sheet of paper was placed 52 meters from the system. At this distance, the sheet of paper occupies a field of view of 5.4 mrad. Images have been registered when the zoom is maximized and when it is adjusted to have an image field of view of approximately 31.6 mrad (see Figure 17).

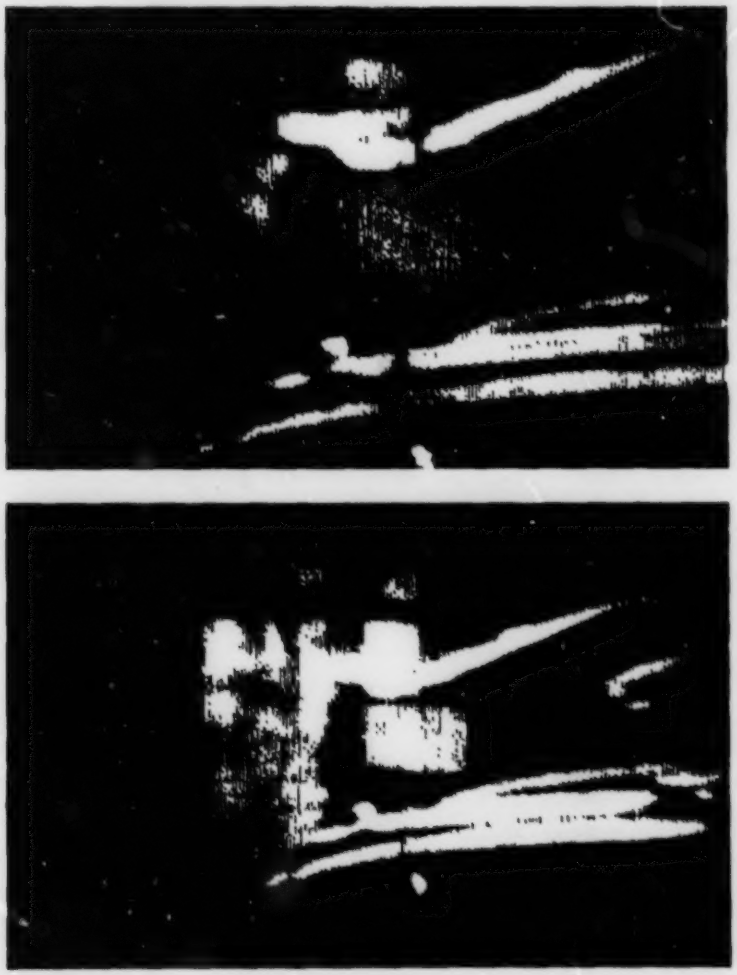

Figure 17: Image of a 8½×11 sheet of paper placed 52 meters from the system when the zoom lens is adjusted to the maximum (top) and when it is adjusted to have a field of view of 35 mrad (bottom). The maximum zoom gives a field of view of approximately 23 mrad.

5.5.2 Beam splitter for the visual channel

The beam splitter for the visual channel has been chosen for good UV transmittance. As a result, it reflects only a small fraction of the incident light, even in the visible range. The beam splitter has been chosen with two different coatings on each side in order to avoid a severe doubling of the reflected image.

The beam-splitter model W2-PW-2025-UV-AR308-BBARVIS-45UNP from CVI Laser is used for operation at 308 nm. Its transmittance at this wavelength is 0.923. Also from CVI Laser, model W2-PW-2025-UV-AR351-BBARVIS-45UNP is used for operation at 351 nm. Its transmittance at this wavelength is 0.940.

5.5.3 UV Filters

Two identical UV filters are placed in front of the visual camera to remove scattered laser radiation. These filters must be replaced when changing the wavelength: the GG375 filters must be used for 351 nm operation while the WG335 are used for 308 nm operation.

5.6 System synchronization

The laser pulses must be synchronized with the collection of photons, both in the backscatter and spectral channels. Three main points must be taken into account for determining an appropriate synchronization scheme.

1. Spectral vectors, obtained from a completed vertical binning of the ICCD camera can be transferred to the computer at a high rate (up to 470 Hz), but only if internal triggering is used. The internal clock of the ICCD camera must then be the master of the system repetition rate.

2. The laser pulses detected by the triggering detector must master the ICCD gating for compensating jitter between the laser trig and the laser pulses.

3. The repetition rate of the ICCD transfer must be twice the one of the laser in order to collect background information between the laser pulses.

These three constraints conducted in the synchronization scheme shown in Figure 20. As can be seen in Figure 20, three electronics circuits have been designed. A first one serves for amplifying the photo-diode current and producing appropriate two identical

TTL output signals. A second one is used for dividing the trig signal from the ICCD camera by a factor of 2, its output being used for triggering the laser. Finally, a third one is used to double the rate of the signal coming from the delay generator. In fact, this last circuit mixes two outputs of the delay generator, delayed from each other of half the time interval between two laser pulses. The repetition rate of the output of the mixing circuit is thus twice the rate of one delay generator output. The first circuit was mounted on a separate board and a separate box while the other two circuits are mounted together on the same board. The divider, mixer and photodiode electronics circuits are reproduced in Figure 18 and Figure 19.

As stated in point 1 above, the data from the ICCD can be transferred at high rate, up to 470 Hz. The laser maximum repetition rate is 200 Hz such that the data from the ICCD must be transferred not faster than 400 Hz. The transfer rate of the ICCD data can be limited by providing a delay between transfers. Unfortunately, this delay must be specified as a certain number of millisecond. A delay of 3 ms must be specified in order to limit the transfer rate to 333 Hz. A delay of 2 ms would result in having a transfer rate larger than 400 Hz.

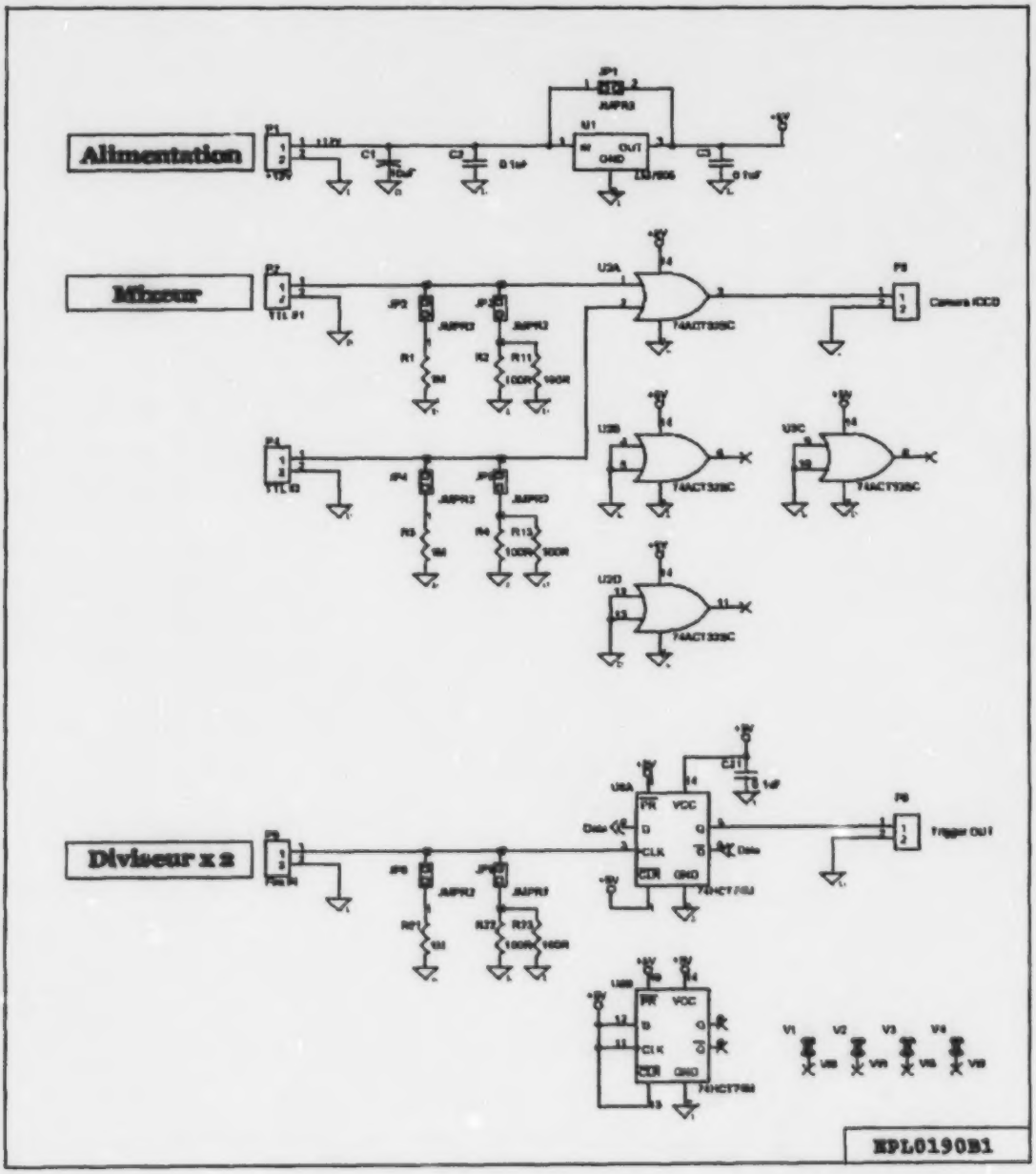

Figure 18. Mixer and divider electronics circuits used for the synchronization of the system.

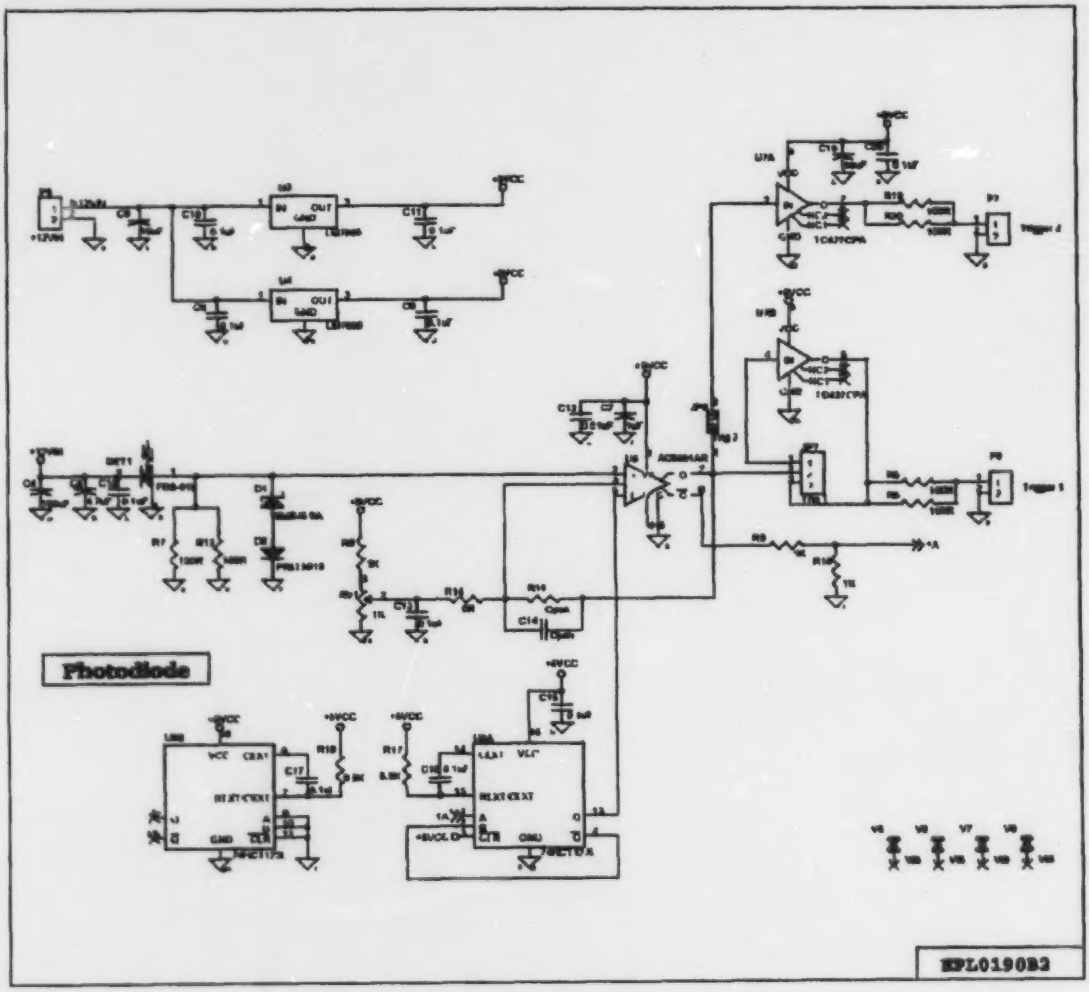

Figure 19: Electronics schematics of the photodiode signal shaping and alimentation.

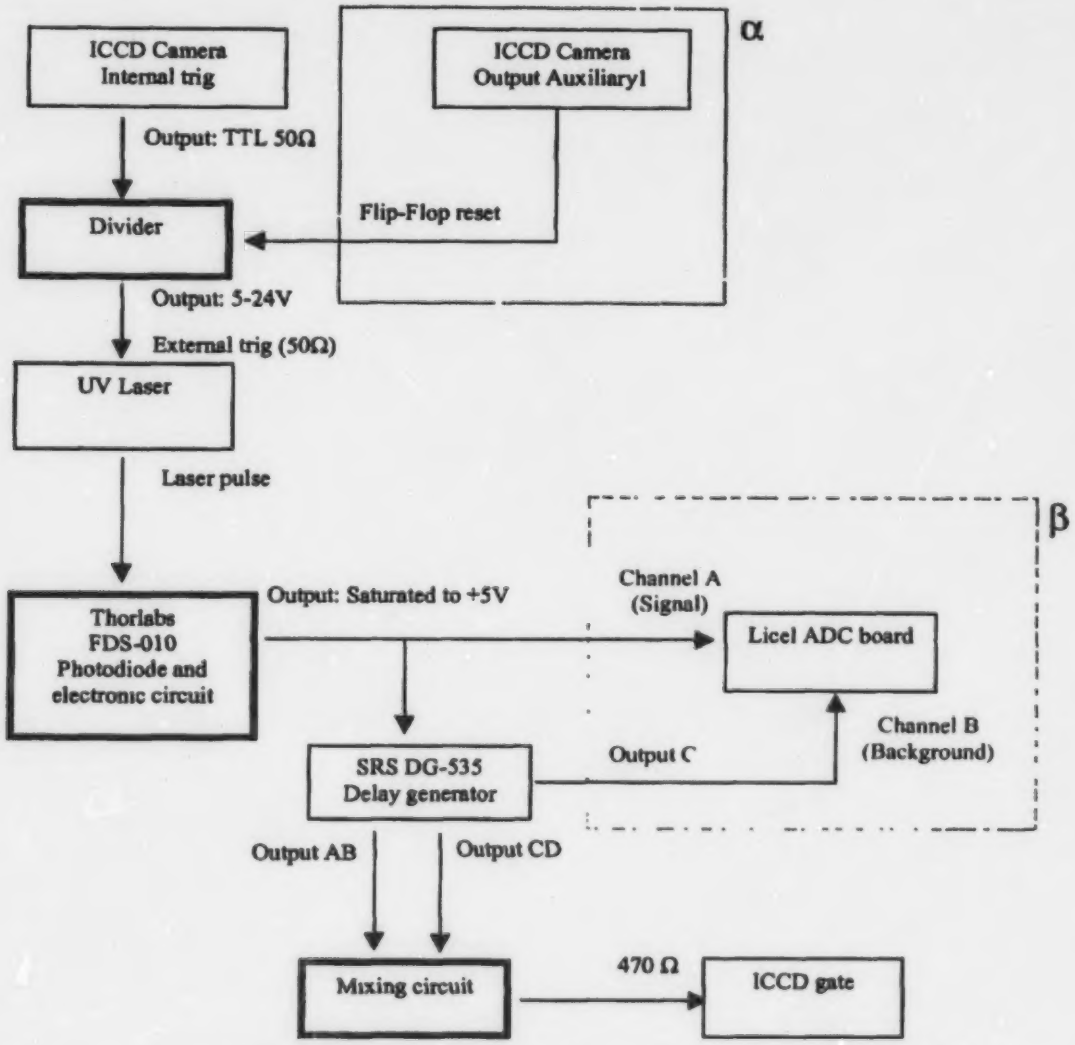

Figure 20: Synchronization scheme between the laser, the ICCD camera and the Licel system. Box noted α has been added to allows resetting of the divider (flip-flop) by software, while box noted β is a modification of the original design to provide backscattered radiation from the Licel in both background and signal mode.

Figure 21 to Figure 24 show typical signals at different points of the synchronization scheme. The actual ICCD transfer rate is 328.5 Hz as can be deduced from Figure 21.

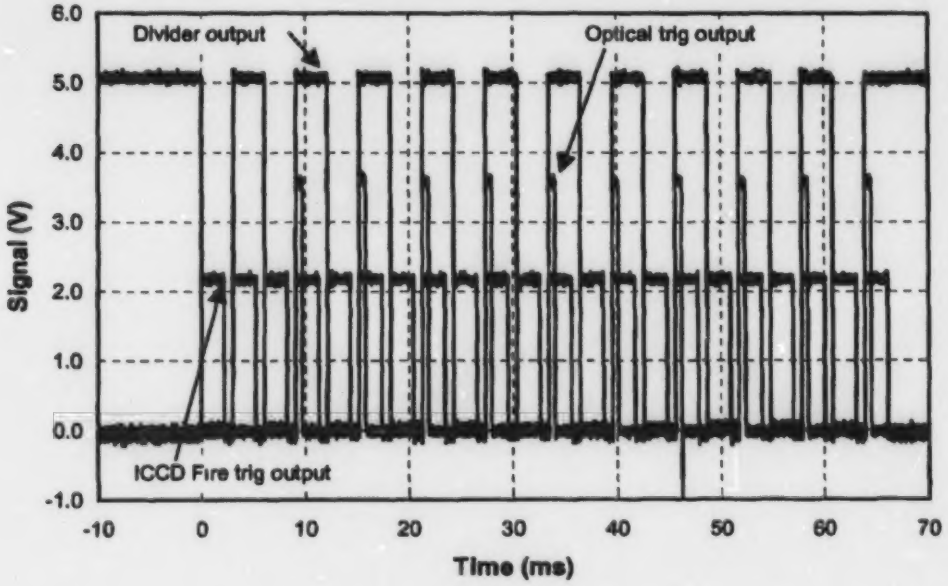

Figure 21: ICCD output trig signal, Divider output signal and Photodiode output signal shown on millisecond time scale when 22 acquisitions are programmed. The first upper front transition sent to the laser serves for initialization while all others trig laser pulses.

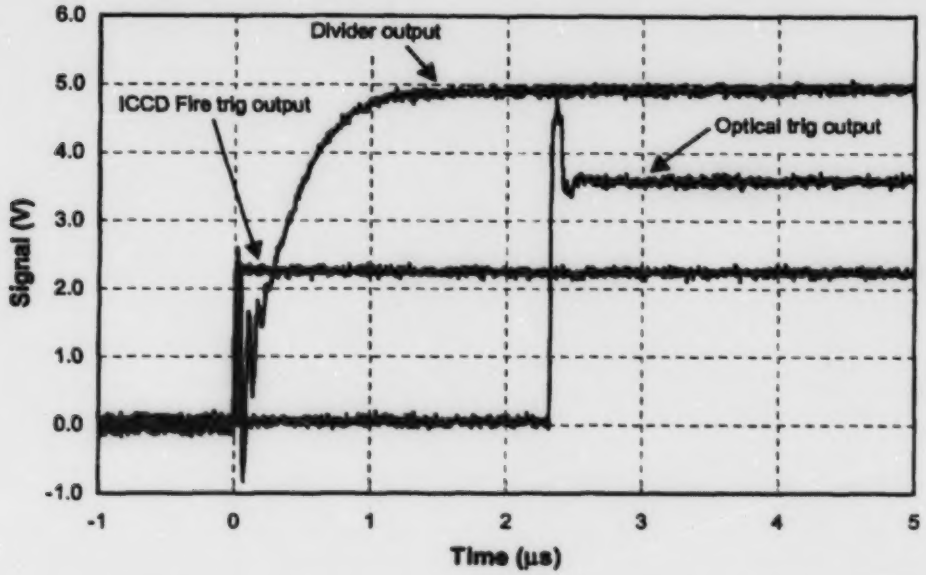

Figure 22: ICCD output trig signal, Divider output signal and Photodiode output signal shown on microsecond time scale

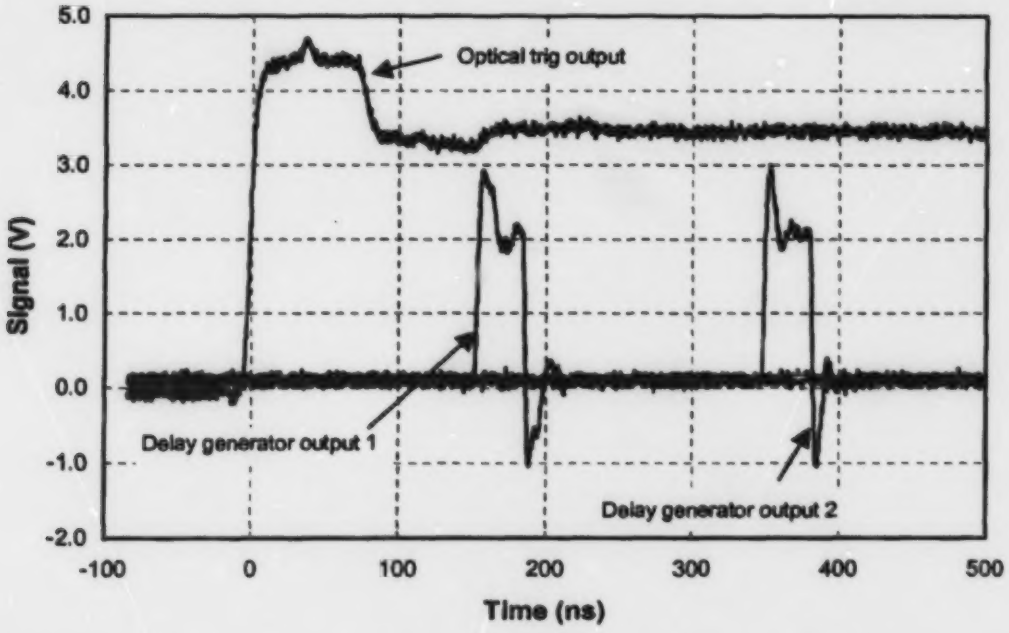

Figure 23: Photodiode output signal, and the two Delay generator outputs shown on the same time scale.

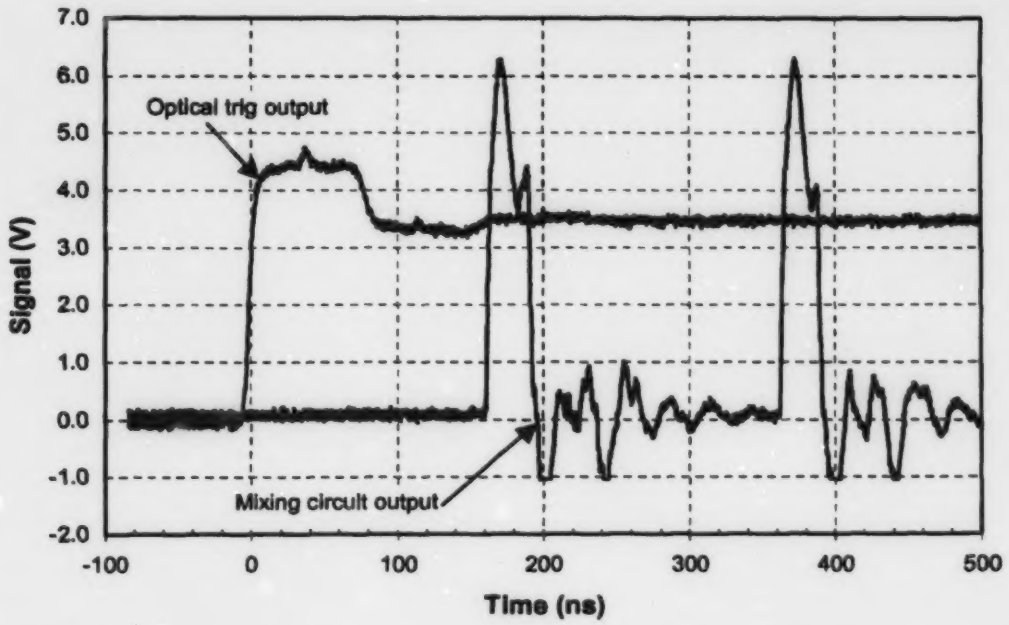

Figure 24: Photodiode output signal and mixing circuit output shown on the same time scale.

5.7 Overlapping functions

The receiving optics of lidar consists of a main primary mirror with a smaller folding mirror that acts as a central obscuration. Backscattered radiation from a given point P in the target plane (illuminated atmospheric layer) at a distance z is focused into the image plane, giving rise to a circle of confusion of radius $r_c = r_{mirr} f/z$ with the inner dark region due to the obscuration with the radius $r_b = r_{central_mirr} f/z$ and shifted from the optical axis of receiving system to the distance $n = r f/z$, where r is the shift of point P at the target plane from the common optical axis of lidar, r_{mirr} is the radius of the primary mirror, $r_{central_mirr}$ is the radius of the secondary mirror, and f is the focal lens of the telescope.

The irradiance in the focal plane could be obtained by integration over all circles of confusion for given field of view of telescope for the radius at the target plane from 0 to $r_t = r_{mirr} + r_{detect}\, f/z$, where r_{detect} is the radius of the detector in the focal plane, and for different values of the distance z, assuming that the laser beam falls into the field of view of the telescope. The Geometrical form – factor or effective area of telescope could be calculated as the ratio between the integral of overlapping function and the real area of the

the surface of main mirror of telescope taking into account the useful surface of detector, calculated as the intersection of the detector area and the area of image of point P for the given distance z. Thus, we can write a geometrical probability factor g as[1],

$$g(z, r_c, r_b, r_{detect}) = \left(S_{inter_detect_rc} - S_{inter_detect_rb}\right) / S_c$$

where $S_{inter_detect_rc}$ and $S_{inter_detect_rb}$ are the area overlap functions for the primary mirror and the secondary (obscuring) mirror respectively, and S_c is the surface of the circle of confusion.

For a distance z, the diameter of laser beam assuming a Gaussian profile, could be calculated as:

$$w^2(z) = w_0^2 + (\varphi_0 z)^2$$

where φ_0 is the tangent of the angle of divergence of the laser, including the laser pointing stability. We can thus write the Geometrical form – factor for the lidar as,

$$\xi(z) = \frac{1}{\pi r_{mirr}^2} \frac{r_{mirr}^2}{w^2(z)} \iint_{S_T} g(z, r_c, r_b, r_{detect}) \cdot \exp\left(-r^2 / w^2(z)\right) r \, dr \, d\phi$$

where S_T is the surface in the target plane, as defined from the telescope field of view.

The results of calculation for $r_{detector} = 4$ mm (for diameter of photocathod of PMT) and for $r_{detector} = 0.1$ mm , for 200 μm width of the slit of spectrometer M260i are shown in Figure 25 and Figure 26.

[1] See Measure, R. M., *Laser Remote Sensing: Fundamentals and Applications*, John Wiley & Sons, New York, 1984, sec. 7.4.2.

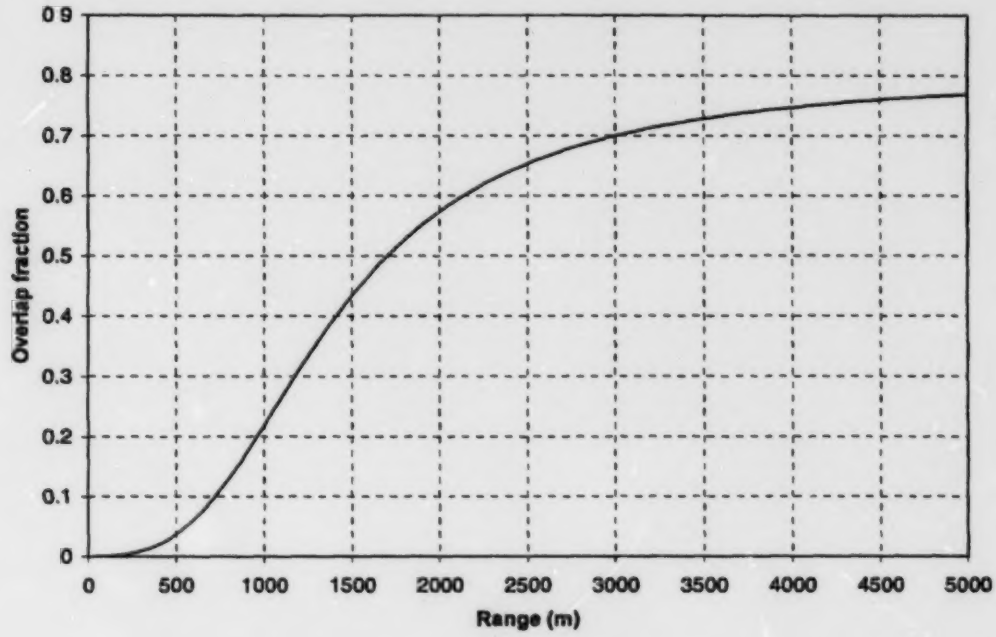

Figure 25: Overlap function between the laser and the spectrometer field of view

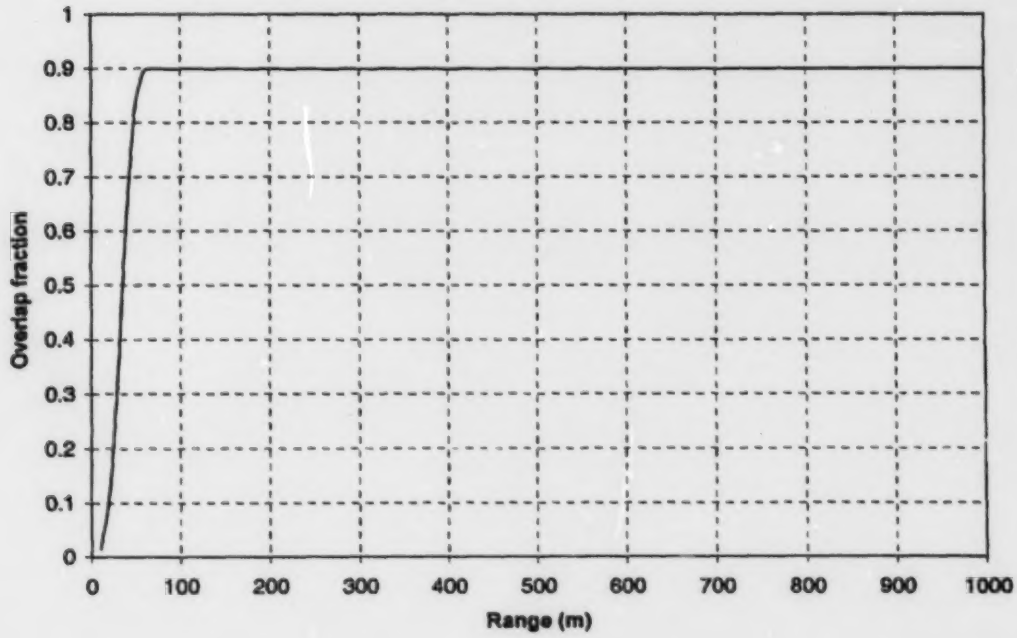

Figure 26: Overlap function between the laser and the backscatter detector field of view.

5.8 Weather monitoring (N.1, N.2, N.3, N.4, O.1)

A weather station model WS-2000 from RainWise and a visibility monitor model 6100 from Belfort are installed on the roof of the trailer for atmosphere characterization. These devices are used to measure the parameters listed in Table 8, which also gives the specifications provided by the manufacturers. The weather station and visibility monitor have been tested by comparing the readings with the data from Environment Canada for Quebec city (Web site http://weather.ec.gc.ca/prevision/yqb.html).

Device	Parameter	Range	Accuracy
RainWise weather station model WS-2000	Temperature	-54 to +74°C	± 1°C
	Atmospheric pressure	551 to 1084 mbar	± 1.69 mbar
	Relative humidity	0 to 100%	± 2% at 25°C
	Wind speed	0 to 67 m/s	± 2% of full scale
	Wind direction	360°	± 3% of full scale
Belfort model 6100	Visibility	6 m to 16 km	± 10% of reading

Table 8: Specifications of the weather monitoring equipment.

Date and hour	Source	Temperature	Atmospheric Pressure	Relative humidity	Wind Speed	Wind direction	Visibility
2000-10-13 9h00	XDM	15°	100.64 kPa	60%	11.3 km/h	-	15 km
	Env. Can.	10.1°	101.46 kPa	80%	20.4 km/h	O	48 km
2000-10-26 11h00	XDM	9°	108.30 kPa	91%	3.2 km/h	ONO	3.2 km
	Env. Can.	10.2°	102.34 kPa	94%	16.6 km/h	O	2.4 km

Table 9: Comparison test of the XDM weather station and visibility monitor with the data from Environment Canada.

6. CALIBRATION

6.1 Data

The quantification of the bioaerosol concentration requires a proper knowledge of the system. Some parameters are intrinsic to the XDM and are referred to as the calibration data. Some other parameters may depend on particular operation conditions and are referred to as the system parameters. Finally, the bioaerosol cross-section is specifically related to the bioaerosol nature and is classified separately. Note that the nitrogen and oxygen Raman cross-sections are considered as part of the calibration data as they are fixed values.

Parameter	Symbol	Corresponding section	Corresponding calibration file
Wavelength	λ	5 2.4	Lambda1 txt, Lambda2 txt, Lambda3 txt
Spectro-ICCD response	$\kappa(\lambda)$	5.2 4	Kappa1 txt, Kappa2 txt, Kappa3.txt
ICCD gain factor	G	5.2 4	ICCD_Gain_G_L1 txt
Spectral channel overlap function	$\xi(r)$	5.7	Overlap_x1_r_q3q4 txt
Backscatter channel overlap function	$\xi_{bs}(r)$	5.7	Overlap_x1_bs_q3q4 txt
Telescope free aperture	A_0	5.2 1	ScalarCalibrationData_308 txt, ScalarCalibrationData_351 txt
Visual camera beam splitter transmittance	$t_{BS}(\lambda)$	5 5.2	ScalarCalibrationData_308 txt, ScalarCalibrationData_351 txt
Beam expander transmittance	$t_{BE}(\lambda)$	5.4 2	ScalarCalibrationData_308 txt; ScalarCalibrationData_351 txt
Laser folding mirror reflectance	$r_{FM}(\lambda)$	5.4.4	ScalarCalibrationData_308 txt; ScalarCalibrationData_351 txt
Steering mirror reflectance	$r_{SM}(\lambda)$	5 1	Steering_mirror_rSM_P1.txt
Telescope transmittance	$t_{TEL}(\lambda)$	5.2.1	Transmission_telescope_tTEL_G4.txt
Backscatter channel beam splitter transmittance	$t_{BC}(\lambda)$	5.3.2	Backscatter_beam_splitter_tBC_H1 txt
UV filters transmittance	$t_F(\lambda)$	5 2.2 (*)	UV_filters_transmittance_tF_J1 txt
Nitrogen Raman cross-section	$\frac{d^2\sigma_N}{d\Omega d\lambda}(\lambda_0,\lambda)$	3.3	RamanN2_reseau1_308 txt, RamanN2_reseau1_351 txt, RamanN2_reseau2_308 txt, RamanN2_reseau2_351 txt, RamanN2_reseau3_308 txt, RamanN2_reseau3_351 txt,
Oxygen Raman cross-section	$\frac{d^2\sigma_O}{d\Omega d\lambda}(\lambda_0,\lambda)$	3.3	RamanO2_reseau1_308 txt, RamanO2_reseau1_351 txt, RamanO2_reseau2_308 txt, RamanO2_reseau2_351 txt, RamanO2_reseau3_308 txt, RamanO2_reseau3_351 txt,
Laser pulse duration	τ_p	5.4.1	ScalarCalibrationData_308 txt, ScalarCalibrationData_351.txt

Table 10: Calibration data

(*): UV Filter transmission values below 5% (occurring at short wavelengths) have been replaced by this value in order to prevent a division by small number resulting in significantly increasing the noise.

Referring to the nomenclature introduced in the previous sections, the calibration data, system parameters and bioaerosol data are listed in Table 10, Table 11 and Table 12. If any, the corresponding calibration file used by the software is given also.

Parameter	Symbol	Typical value
Number of laser pulses per acquisition	n_{pu}	1000
Pulse energy	E_d	150 mJ
ICCD gate duration	τ_g	20 ns
Range	r	50 – 5000 m

Table 11: System parameters

Parameter	Symbol
Bioaerosol cross-section	$\frac{d^2\sigma_{ba}}{d\Omega d\lambda}(\lambda_0,\lambda)$

Table 12: Reference data

6.2 Calibration procedure

There is no calibration procedure for upgrading the calibration data since they are not expected to change over time. However, the laser energy reading has to be re-calibrated from time to time. This can be done using a calibrated power-meter as described in the Lumonics laser calibration procedure.

There is a calibration procedure for obtaining the bioaerosol cross-section. This procedure is available through a functionality of the software and is described in the Software User Manual INO 99-5217SM R N/A.

7. TESTS OF THE SYSTEM IN THE FIELD

7.1 Backscatter channel

7.1.1 Test with no target: Rayleigh scattering

Backscattered light has been recorded when the lidar is directed in the air in a region where no obstacle appears in the field of view. Figure 27 shows the resulting signal with and without the application of the preprocessing[2]. The usual $1/r^2$ signal from the Rayleigh and aerosol scattering is observed on the raw signal. The preprocessing properly remove this range dependence. The PMT voltage was set to 650 V for this analog measurement.

[2] Note that for Figure 27 and Figure 28, some points that were causing regular steps in the curve have been removed from the original data. Their origin is unknown but since the system now behave properly, they are believed to come from a bad electrical connection during the measurement.

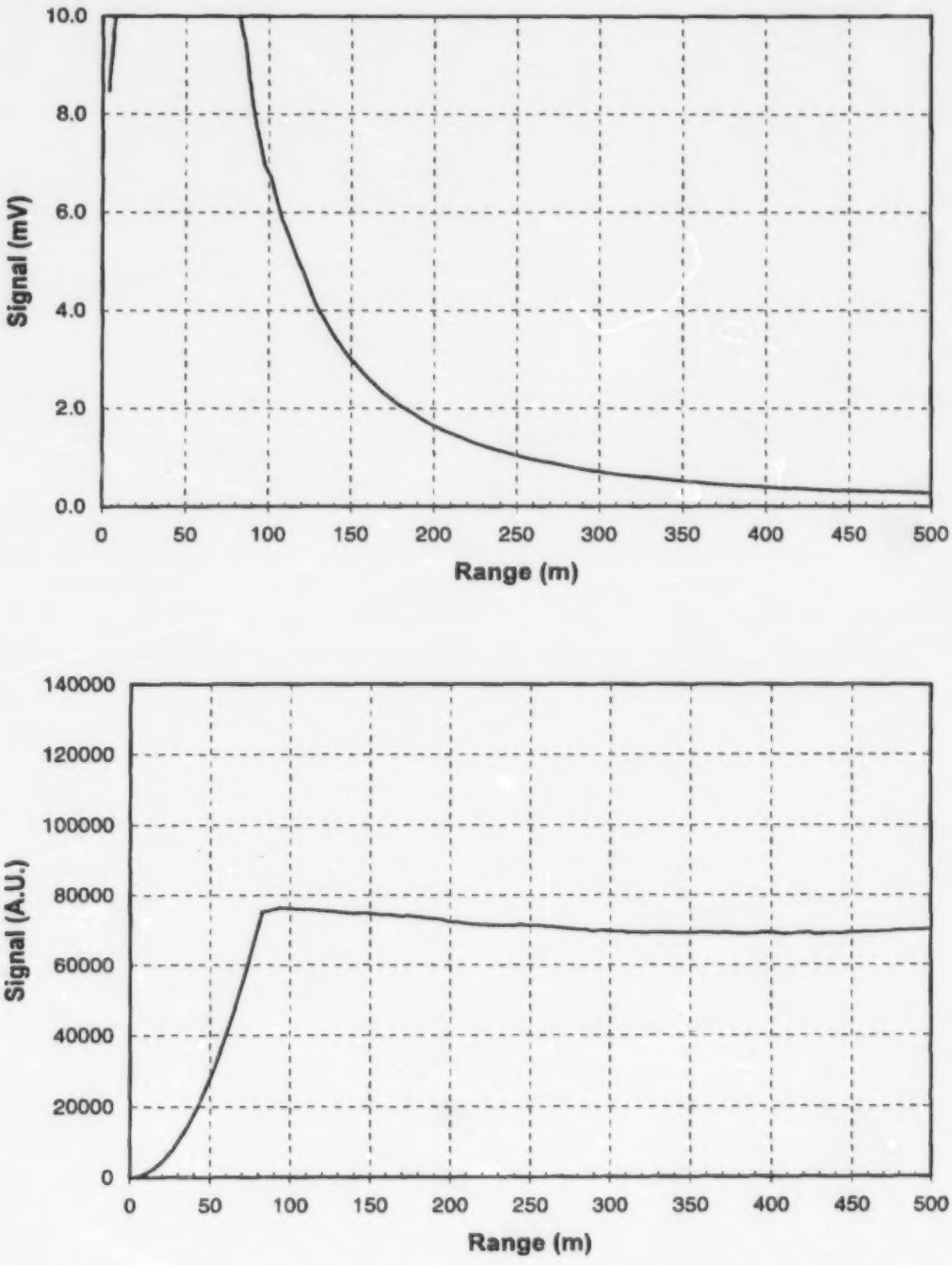

Figure 27: Backscatter signal recorded when the lidar is directed towards the sky (no obstacle present). Raw signal (top) and preprocessed signal (bottom).

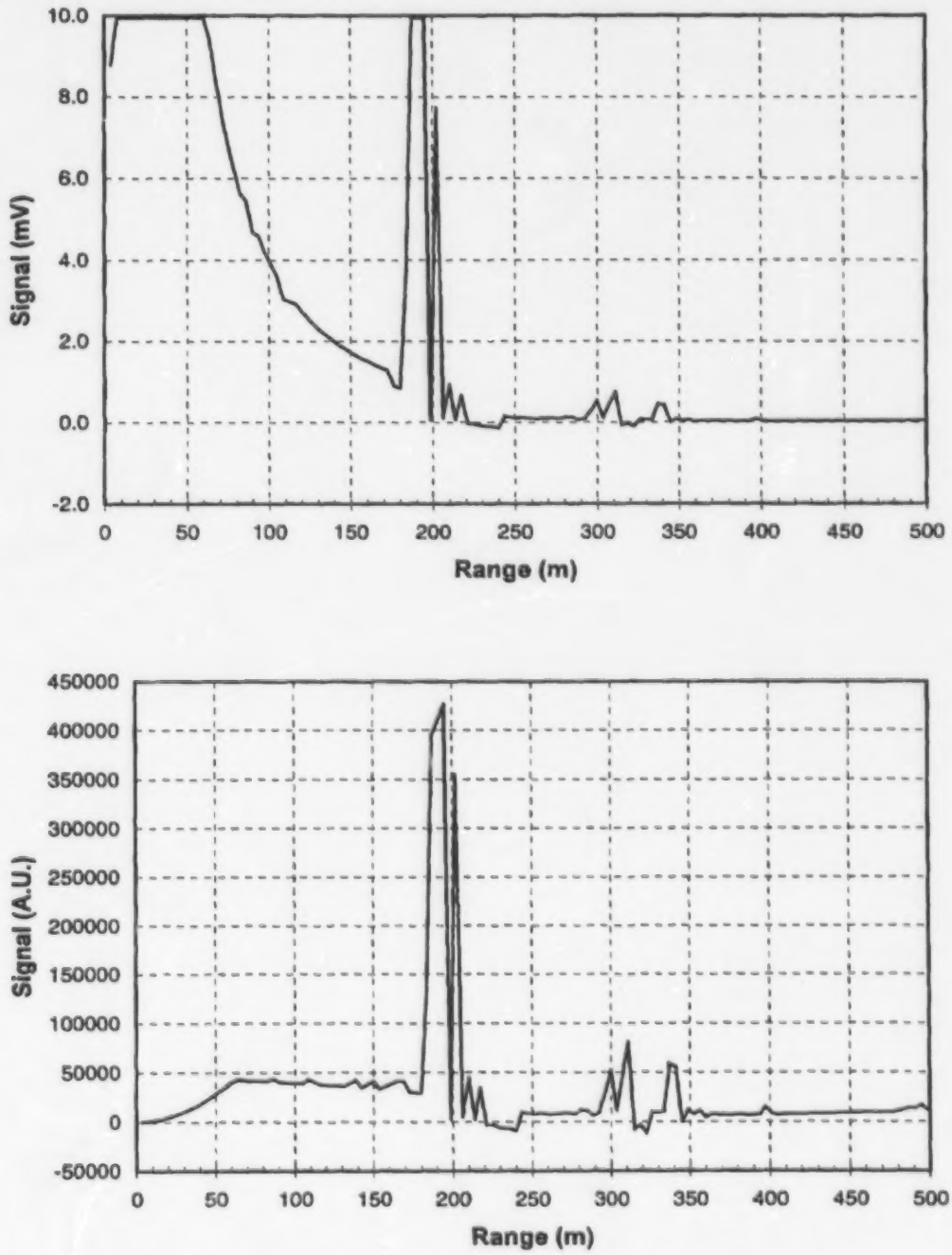

Figure 28: Backscatter signal recorded when the lidar is directed towards a solid target placed at 183 m from the trailer. Raw signal (top) and preprocessed signal (bottom).

7.1.2 Test with a solid target

The lidar was directed towards a solid target placed at 183 meters from the trailer. Figure 28 shows the resulting recorded signal with and without the application of the preprocessing. As expected, a strong peak is observed at the proper range. Obviously, the range-independent background on the preprocessed signal is significantly decreased after the target. The PMT voltage was set to 600 V for this analog measurement.

7.2 Spectral channel

7.2.1 Background from day light

A spectral signal was recorded when the laser pulses do not exit the trailer. In that case, only the background from day light can be collected by the spectral channel. Figure 29 shows the resulting signal. Of course, the application of background subtraction results in obtaining only a noisy trace centered on zero.

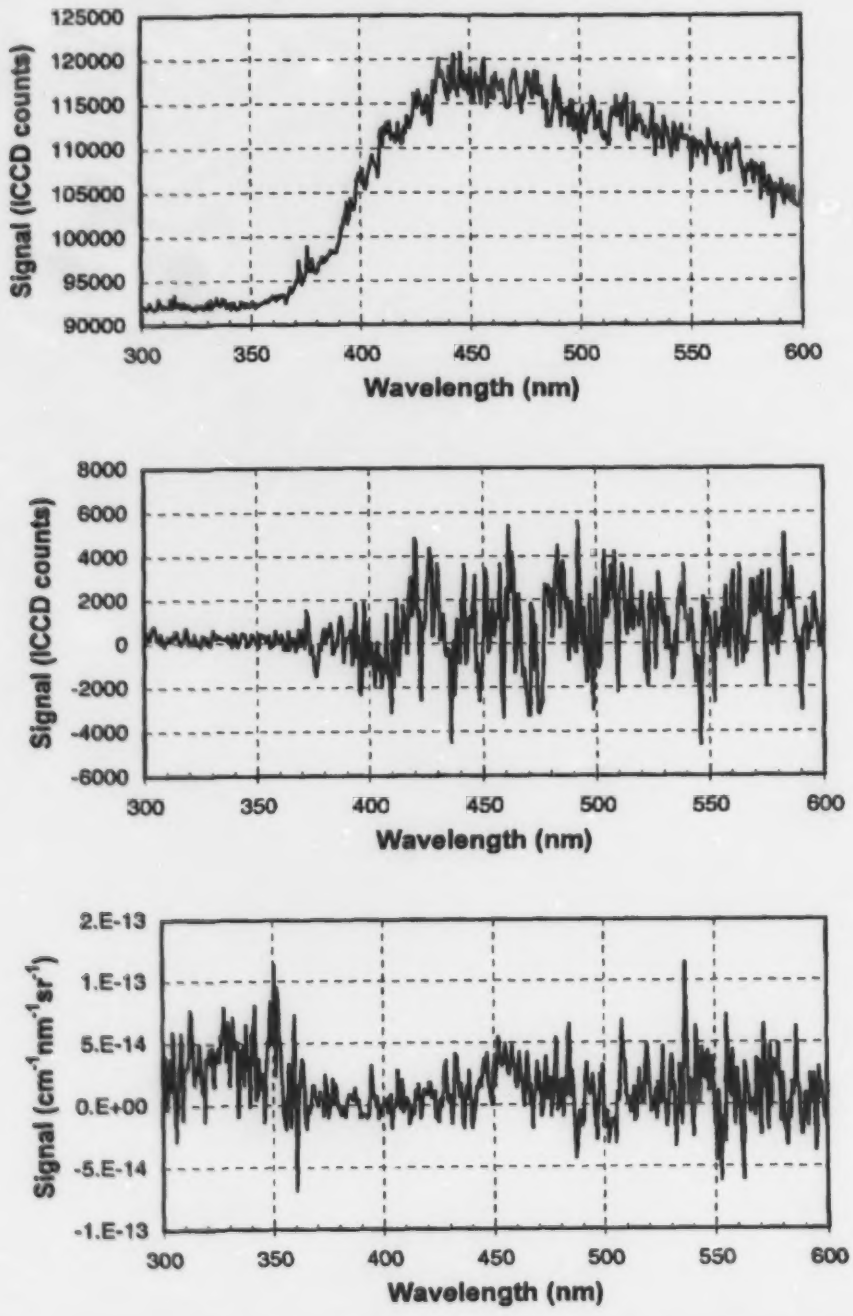

Figure 29: Background from day light when neither the background subtraction and preprocessing is applied (top), when only background subtraction is applied (center) and when both background subtraction and preprocessing is applied (bottom).

7.2.2 Signal from a solid target

The spectral signal from a solid fluorescent target (white cotton) placed at 100 meters from the trailer was recorded when the laser pulses cause it to fluoresce. Figure 30 shows the resulting signal when the range is adjusted to coincide with the target. As can be seen, in that case, the signal is very strong compared to the background light. Note that this measurement was done during the day (about 10h00 in the morning) and the ICCD temperature was set to room temperature. The small peak at approximately 360 nm on the preprocessed graph is an artifact due to the division by the UV filters transmittance. **Values below 360 nm must be considered non-calibrated and non-reliable.**

Figure 31 shows the same result when the range is not adjusted to coincide with the target but is rather placed elsewhere. As expected, the obtained signal in that case is the same that the one obtained with no laser that is only background day light as in Figure 29.

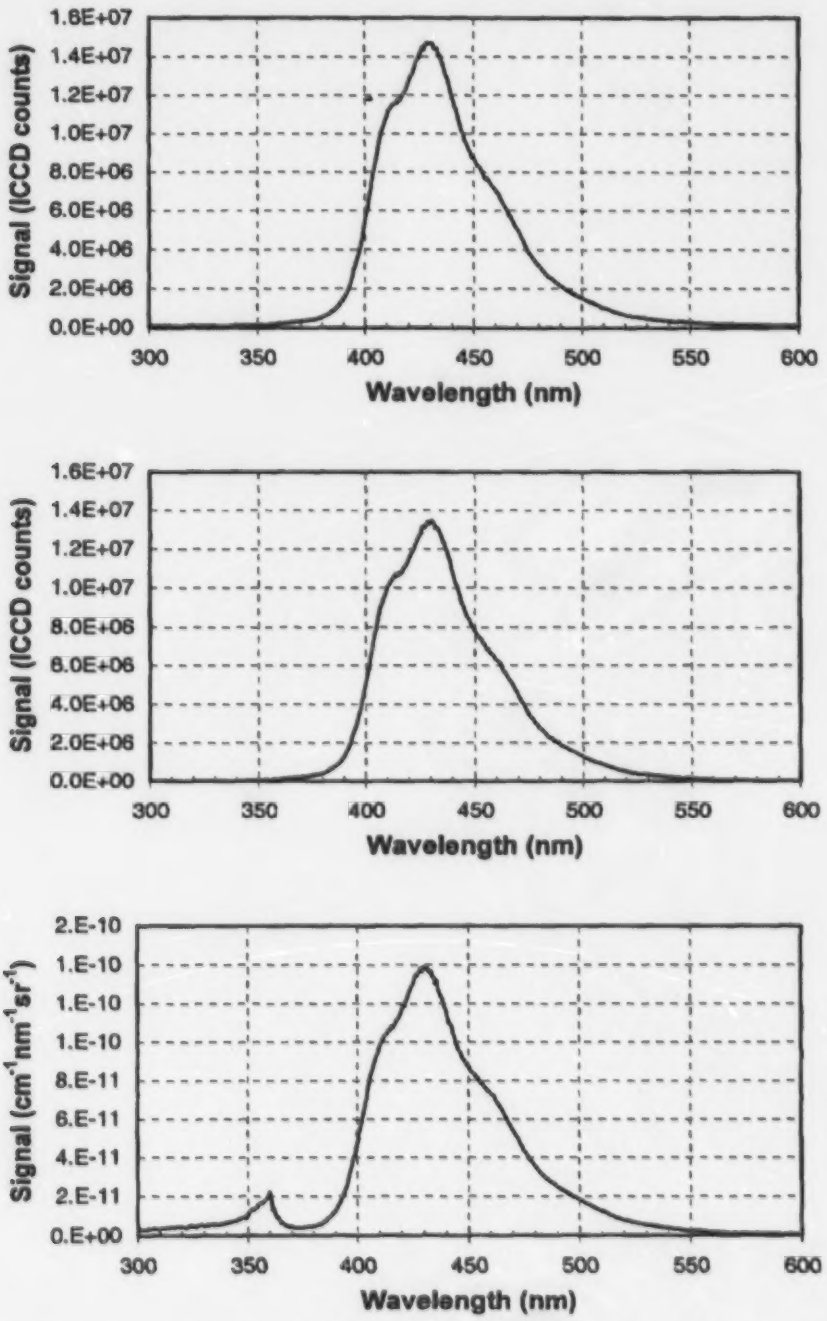

Figure 30: Spectral signal from a solid target placed at 100 meters from the trailer when neither the background subtraction and preprocessing is applied (top), when only background subtraction is applied (center) and when both background subtraction and preprocessing is applied (bottom). These results have been obtained when the range is adjusted to coincide with the target.

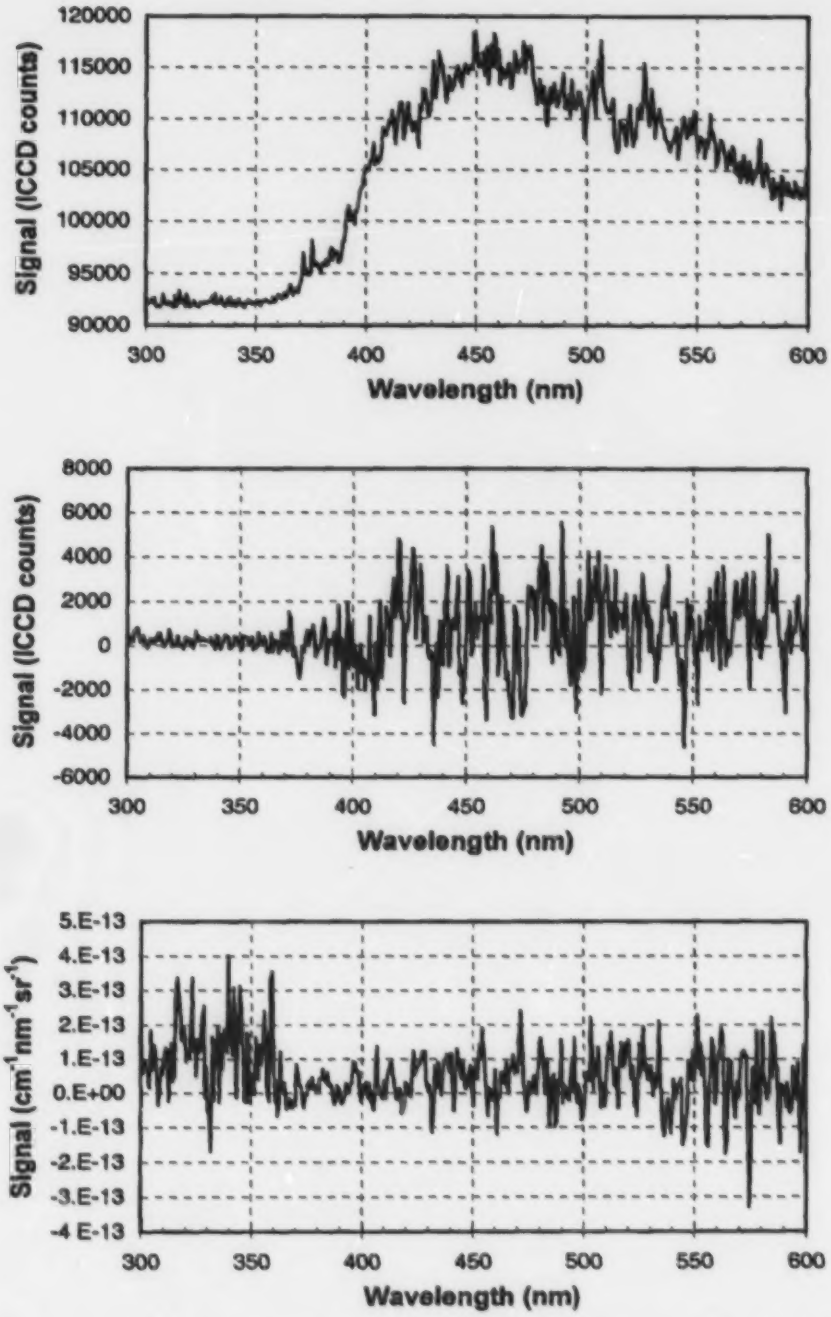

Figure 31: Spectral signal from a solid target placed at 100 meters from the trailer when neither the background subtraction and preprocessing is applied (top), when only background subtraction is applied (center) and when both background subtraction and preprocessing is applied (bottom). These results have been obtained when the range is adjusted to 200 m (no coincidence with the target).

7.2.3 Pre-processing and processing

The cotton target was characterized as if it would be a bioaerosol. A spectral signal has been recorded as being a bioaerosol signature when a strong averaging was applied (4000 pulses) and an arbitrary "known" concentration was set to 1.

Then, a further measurement was done using this cotton signature for processing and all the same system parameters except for the number of laser pulses, which were reduced to 100. A bioaerosol concentration of 0.87 was obtained. A value close to 1 was expected, differences might be due to atmosphere characterization changes from measurement to measurement.

The proper operation of preprocessing was minimally verified by changing some of the system parameters (ICCD gain, spectrometer grating) and performing the same processing. Figure 32 shows the resulting spectral signals in comparison with the fitted cotton profile. In these three cases, bioaerosol concentration between 0.85 and 0.87 have been obtained.

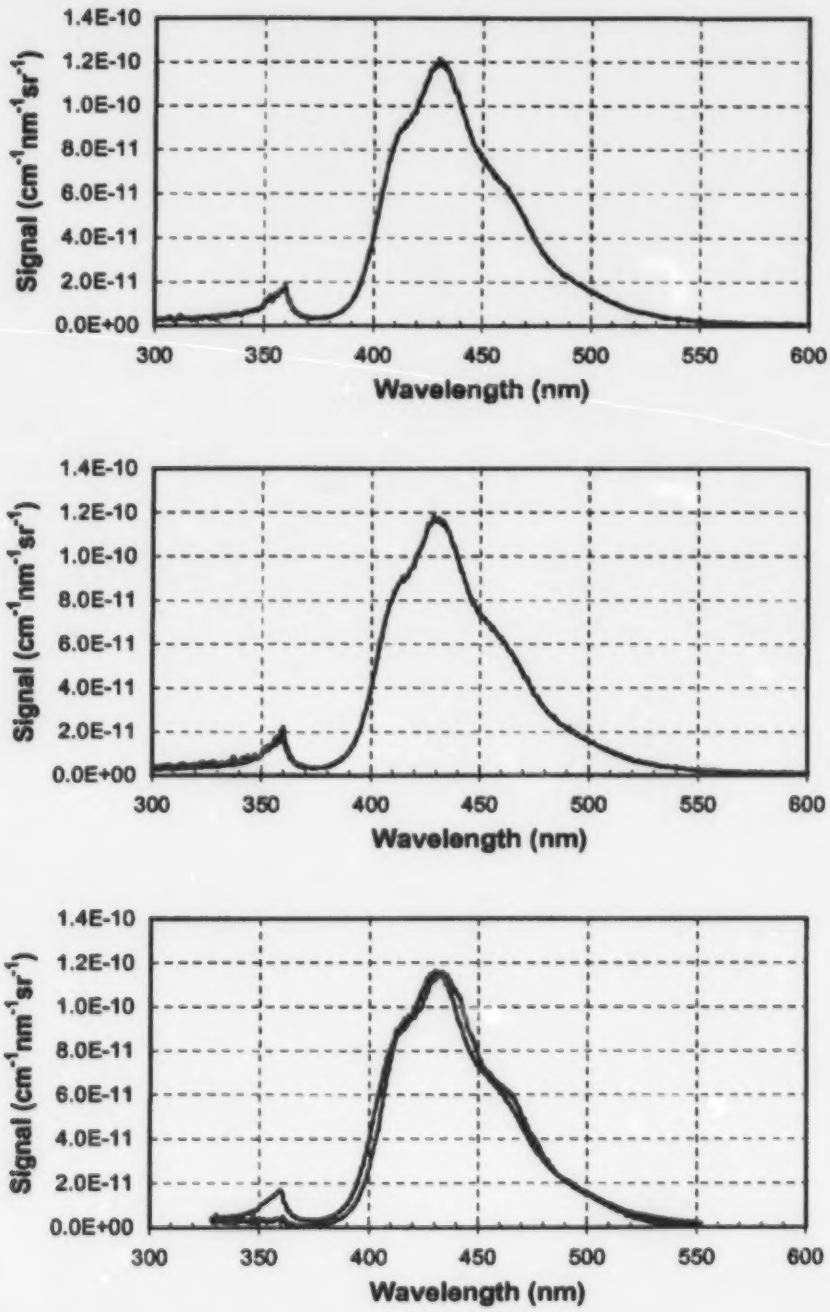

Figure 32: Preprocessed spectral signals obtained in the same conditions but using different system parameters: 1) ICCD gain 9, grating #3, 2) ICCD gain 7, grating #3, 3) ICCD gain 9, grating #2. The fitted cotton signature is also shown (superimposed on the signal).

7.2.4 Signal from the solid target placed at another distance

The cotton target was displaced to 183 meters from the trailer. The signal shown in Figure 33 was obtained resulting in a bioaerosol concentration of 0.34. This low value (expect to be again close to 1) may be due to improper alignment or to an improper characterization of the overlap function. This last quantity $\xi(r)$ was determined theoretically, but for low value of the range (less than 500 m), the calculation result of 0 was replaced by the arbitrary small number 0.0001. A better determination of $\xi(r)$ for small range value could be based on the Raman signals measured in a very clear day (such that the atmosphere transmittance can be approximated to 1 up to 1 or 2 kilometers).

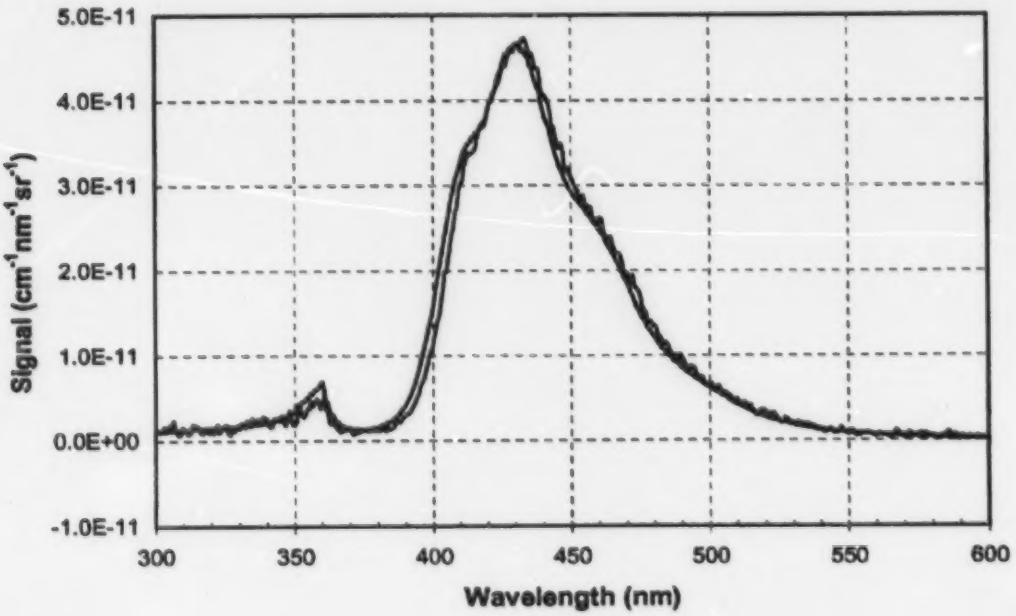

Figure 33: Preprocessed spectral signal obtained from the cotton target placed at 183 meters from the trailer. The fitted cotton signature is also shown.

7.2.5 Raman signals

7.2.5 Raman signals

An unsuccessful trial for detecting Raman scattering was conducted[3]. For that purpose, the lidar was directed towards the sky, in a region where no obstacle is in the field of view. The probed cell was set to a very large value, from 100 to 1000 m. The resulting ICCD signal (with background subtraction but no preprocessing) is shown in Figure 34. Note that the signal without background subtraction was larger than 60000 counts. The ICCD camera temperature was decreased as far as possible that is down to -18°. Spectrometer grating 1 was used for this trial. The ICCD gain was set to 4 and the signal was processed in analog mode. The maximum number of integrated laser pulses (4000) was used. The Raman signals are at 371 and 382 nm for the oxygen and nitrogen respectively.

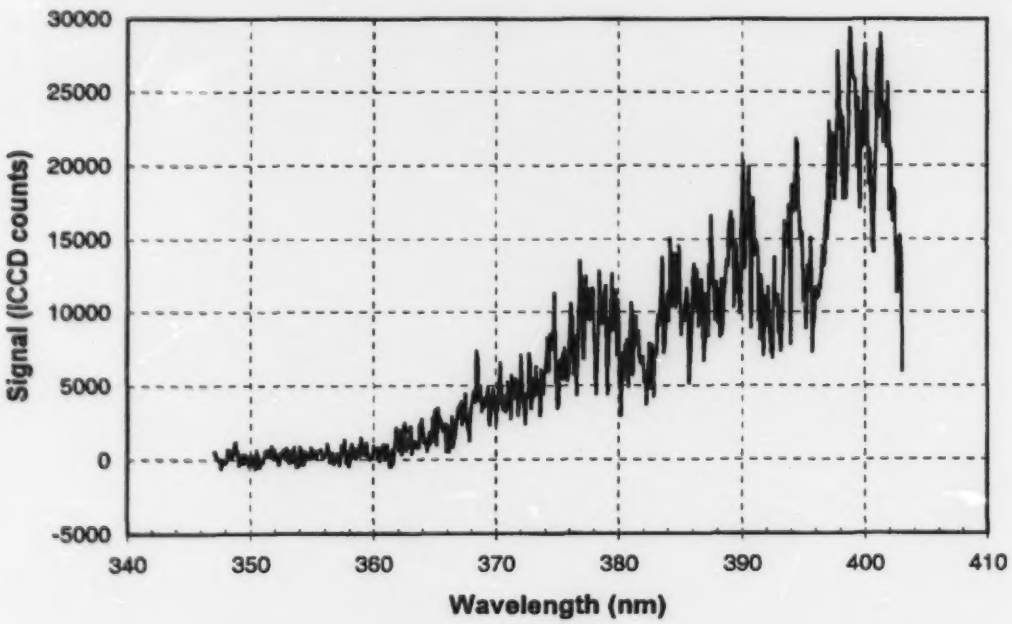

Figure 34: Spectral signal measured with grating 1 when the laser beam is directed towards the sky.

[3] The client recently reported successfully measuring Raman signals after system realignment.

8. ALIGNMENT PROCEDURES

When the XDM is moved to another location, the procedures described in sections 8.2 and 8.3 must be performed. If the lasing wavelength changed with respect to the last use, the elements listed in section 8.1 have to be changed before the procedure described in section 8.3 being performed.

8.1 Changing the wavelength

When changing the laser wavelength of operation, the element listed in the above subsections must be changed.

8.1.1 Visual camera beam splitter

The visual camera beam splitter must be replaced. The beam-splitter model W2-PW-2025-UV-AR308-BBARVIS-45UNP from CVI Laser must be used for operation at 308 nm, while model W2-PW-2025-UV-AR351-BBARVIS-45UNP must be used for operation at 351 nm.

8.1.2 Visual camera UV filters

Two filters are placed in front of the visual camera. They have to be replaced when changing the laser wavelength of operation. The GG375 filters must be used for 351 nm operation while the WG335 are used for 308 nm operation.

8.1.3 Spectrometer UV filters

Two filters are placed in front of the spectrometer. They have to be replaced when changing the laser wavelength of operation. The GG375 filters must be used for 351 nm operation while the WG335 are used for 308 nm operation. The filters can be accessed by slightly sliding the spectrometer in the direction opposite to the telescope, and removing the aluminum black box between the spectrometer and the telescope. The filters are directly attached to the spectrometer.

8.1.4 UV transmitting filter for the backscatter channel

A filter is placed in front of the PMT for transmitting only UV radiation. The filter model F10-350.0-4-0.5 must be used for the operation at 351 nm while model F10-307.1-3-0.5 is used for the laser operation at 308 nm. To access the filter, the black box between the telescope and the spectrometer must be demounted. Then, the mechanical apparatus in front of the PMT must be demounted in a room having only a very weak lightening.

8.1.5 Beam expander

The first lens of the beam expander must be moved to adjust the distance between the two lenses according to the values shown in Table 13.

Laser wavelength	First lens nominal position
308 nm	414.902 mm
351 nm	422.722 mm

Table 13: Theoretical distance required between the two lenses of the beam expander for the two laser wavelengths of operation.

8.2 Weather station

When installing the weather station in its post, the Solar cells must be orientated directly to the south to ensure a proper measurement of the wind direction.

8.3 Lidar alignment

Basically, as long as the entrance slit of the spectrometer faces the telescope output port and is positioned to the desired longitudinal location, the spectrometer is considered aligned: the other three channels are to be aligned with respect to it.

The procedure for aligning the four channels together is the following:

1. Position the spectrometer to the desired longitudinal location (see details in section 8.3.1).

2. Place a laser pointer in the field, at least 50 m from the trailer and align it so that it points to the center of the steering mirror (less than 100 m may render the alignment easier). The laser pointer must be kept turned on up to step 10. The laser pointer can be attached to a mount having two angular adjustments. This mount can be attached to a camera tripod.

3. Remove the spectrometer cover.

4. Open the spectrometer entrance slit to 3 mm.

5. Using the Sinbahd Software, open the spectrometer shutter.

6. Using the joystick, find the steering mirror angular position such that it roughly maximizes the laser pointer power entering the spectrometer. A white card located inside the spectrometer just after the entrance slit might help to achieve this alignment. To render this procedure easier, a preliminary adjustment of the steering mirror can be done by placing a white card in the center of the telescope output port and finding the steering mirror angular position that centers the laser pointer beam on it.

7. Close the spectrometer entrance slit to 200 μm (about 210 on the micrometer reading according to the calibration discussed in section 5.2.3) and repeat step 6.

8. Using the Sinbahd Software, fine tune the steering mirror angular position such that the spectral signal is maximized. At this step, the spectrometer field of view can be considered centered on the laser pointer.

9. Adjust the laser folding mirror angular position such that the laser pointer beam is centered on the UV laser output port. For that purpose, first unscrew the three locking screws (those having a series of springs). Then angular adjustment will be possible by turning the upper left and lower right adjustment screws.

10. Place a solid fluorescent target in front of the laser pointer. Mark the point on the solid target illuminated by the laser pointer beam. Report this point to the opposite side of the solid target (with a precision of about 1 cm).

11. Turn off the laser pointer.

12. Turn on the UV laser.

13. Adjust the laser folding mirror such that the UV laser beam hits the target (a fluorescent spot could be visible).

14. Adjust the beam expander first lens longitudinal position such that the dimension of the fluorescent spot on the target is minimized. Upgrade the value of Table 13: the adjusted longitudinal position of the lens must be considered as the new nominal position for this laser wavelength.

15. Adjust the laser-folding mirror such that the mark on the solid target is centered on the fluorescent spot caused by the UV beam.

16. Using the Sinbahd Software, fine tune the laser folding mirror angular position such that the spectral signal is maximized. Then secure the folding mirror angular position by tightening the three locking screws.

17. Using the Sinbahd Software, fine tune the position of the Licel PMT detector such that the backscatter signal is maximized.

18. Turn off the UV laser (or just stop lasing).

19. Slightly displace the CCD visual camera such that the mark on the solid target is centered on the CCD image. Adjust focus an zoom.

8.3.1 Longitudinal position of the spectrometer

By moving the spectrometer longitudinally, the entrance slit can be placed at the image plane for a specific object plane. In that case, one considers that the spectrometer position is optimized for a range that corresponds to this specific object plane. The back focal length of the telescope is 113.28 mm: placing the entrance slit plane (which corresponds to the center of the slit micrometer) at 113.28 mm from the telescope output port surface thus optimizes the light collection for an object place at an infinite distance from the trailer. Table 14 gives the spectrometer position as a function of the optimized range. The values of Table 14 have been calculated according to the following lens equation:

$$Z = \frac{1612.9}{r_0 - 1.27} + 113.28\,\text{mm}, \qquad (21)$$

where r_0 is the optimized range in meters and Z is the spectrometer position defined as the distance between the telescope output port surface and the spectrometer slit plane (centered on the micrometer center).

Optimized range	Spectrometer position
Infinity	113.28 mm
5000 m	113.60 mm
4000 m	113.68 mm
3000 m	113.82 mm
2000 m	114.09 mm
1000 m	114.89 mm
500 m	116.51 mm
300 m	118.68 mm
200 m	121.40 mm
100 m	129.62 mm
75 m	135.16 mm
50 m	146.38 mm

Table 14: Spectrometer position as a function of the optimized range. The spectrometer position is defined as the distance between the telescope output port surface and the spectrometer slit plane (centered on the micrometer center).

The spectrometer can be translated longitudinally by unlocking the four knobs that secure the spectrometer lower plate on the optical table and by using either the coarse (black anodized aluminum) or fine (brass) translation support. The translation is achieved due to the use of a differential knob. The step per turn is given in Table 15 for both the coarse and fine translation support. Once the translation is achieved, the four knobs must be tighten.

Translation support	Step
Coarse	1.1571 mm / turn
fine	0.0635 mm / turn

Table 15: Step per turn for the two translation supports.